

Robot Body Schema Learning from Full-body Extero/Proprioception Sensors

Shuo Jiang, Jinkun Zhang, Lawson Wong

Abstract—For a robot, its body structure is an *a priori* knowledge when it is designed. However, when such information is not available, can a robot recognize it by itself? In this paper, we aim to grant a robot such ability to learn its body structure from exteroception and proprioception data collected from on-body sensors. By a novel machine learning method, the robot can learn a binary Heterogeneous Dependency Matrix from its sensor readings. We showed such matrix is equivalent to a Heterogeneous out-tree structure which can uniquely represent the robot body topology. We explored the properties of such matrix and the out-tree, and proposed a remedy to fix them when they are contaminated by partial observability or data noise. We ran our algorithm on 6 different robots with different body structures in simulation and 1 real robot. Our algorithm correctly recognized their body structures with only on-body sensor readings but no topology prior knowledge.

Index Terms—Kinematics, robot body schema, graph theory, machine learning

I. INTRODUCTION

As individuals, humans possess an innate understanding of their bodily configuration characterized by the interlink of four limbs, a central trunk, and a head. Within the human nervous system, the somatosensory cortex plays a central role in the apprehension of such body schema. This term denotes the personal awareness of their body, encompassing precise cognition of their temporal and spatial interrelationships of body parts, and the holistic functional integrity [26, 27]. The establishment and maintenance of this schema relies on exteroception and proprioception signals acquired from receptors distributed throughout the body. Exteroception encompasses sensory information originating from external sources, including tactile, visual, auditory, olfactory, and other sensory modalities. Proprioception perceives internal body movement and its spatial orientation. The somatosensory cortex synthesizes these incoming sensory signals into a comprehensive representation of the entire body, which encapsulates essential aspects such as the body's topological structure, sensory receptor distribution, posture, and gestures [28, 24].

With the advancement of AI in robotics, we are actively exploring the role of AI in augmenting a robot's environmental and self-awareness, which encompasses the development of novel perception mechanisms and algorithms. We have observed an increasing adoption of whole-body sensors by a

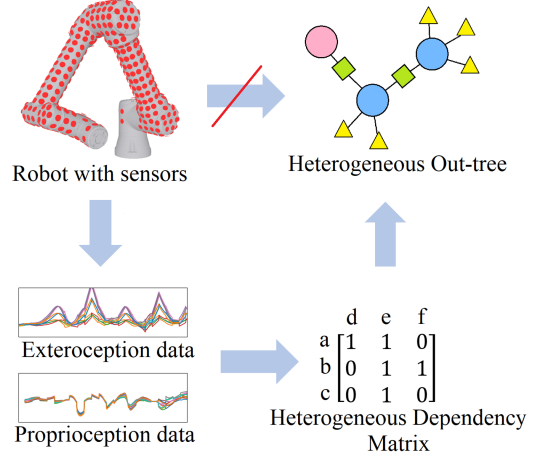


Fig. 1: System flowchart: we cannot directly observe robot topology (represented by heterogeneous out-tree), but we can infer it by extracting a heterogeneous dependency matrix from exteroception and proprioception data and use the matrix-tree equivalence to infer the unobserved tree structure.

diverse range of robots, enabling them to perform tasks such as motion safety [29] and object recognition [30]. Concurrently, the proliferation of diverse robot morphologies, exemplified by the emergence of reconfigurable robots, has introduced heightened complexities in modeling and kinematic analysis. Motivated by the principles of biological body schema learning, we attempted to propose innovative machine learning theories and algorithms for robot body schema learning, which has been less explored. These innovations are aimed at endowing robots with the capability to autonomously perceive their current body structures in real-time, leveraging information gathered from exteroceptive and proprioceptive sensors distributed across their bodies. The concept of our proposed solution is depicted in Fig. 1. We assume that the robot's body schema can be effectively described by a heterogeneous out-tree structure on the interconnections among joints, links, and sensors. However, this underlying topology cannot be directly observed (e.g. by ego-centric vision). To overcome this limitation, we employ an array of exteroceptive sensors, such as Inertial Measurement Units (IMUs), and proprioceptive sensors like joint encoders positioned on the robot's body. Through analysis of the sensor data, we can extract a heterogeneous dependency matrix that encapsulates critical information pertaining to the robot's topology. By means of a rigorous equivalence analysis between this matrix and the out-tree structure, the robot's body schema (in the form of the

out-tree) can be implicitly discerned.

II. BACKGROUND

Evidence has substantiated the notion that humans maintain a comprehensive body representation within their brains [16]. This representation effectively maps multi-modal sensory inputs, such as tactile, visual, and proprioceptive cues, to the spatial poses of various body parts. Within robotics, the concept of body schema demonstrates an intricate interplay with kinematic identification processes. The acquisition and maintenance of a body schema assume paramount importance, particularly when a robot undergoes alterations in its body morphology due to mechanical failures, repair, or material fatigue. The body schema, in this context, endows the robot with the capacity to discern the morphological alteration and facilitate real-time adjustments in the corresponding body control strategies. This adaptive capability is instrumental in averting potentially catastrophic consequences. For a more comprehensive summary robot body representation, readers can refer to the work by [17].

In the study by [21], a Bayesian approach was introduced for the estimation of body schema based on readings from distributed tactile sensors. Their methodology involved an extension of Dirichlet process Gaussian mixture models (DPGMM) [23], which clusters sensor data while simultaneously learning a latent tree structure that represents the robot's body topology. With their approach only relied on exteroceptive information, our framework assumed that proprioceptive data also encodes crucial information about body structure, offering the potential to simplify the inference process. Additionally in their work, accessing global position and velocity data for each sensor can pose challenges in real-world, which is typically supported by a network of costly base stations [10]. This limitation also constrains vision-based systems, as evidenced in prior research [5, 31]. For instance, [5] developed a Bayesian network to model the forward and inverse kinematic structure of a robot that established the relationship between action commands and body poses. This system relied on vision trackers attached to various links, providing 6-D pose information for inference. Nevertheless, the vision tracking approach was reported with self-occlusion issues. [31] employed five depth cameras situated around the robot, in conjunction with joint encoders, to learn the mapping from joint angles to robot morphology. However, their approach focused on learning the robot's body shape, without addressing the topological aspects. Furthermore, [3] introduced an evolutionary algorithm for body schema identification. Their approach utilized multi-modal sensor data, including foot-tip touch sensors, tilt sensors, and body clearance sensors. Their study demonstrated the successful identification of the body structure of a quadrupedal robot but did not present theoretical validation.

III. METHOD

As our goal is to learn the body structure from exteroception and proprioception data, in subsection III-A, we will use the two data sources to learn a proposed global pose for each sensor. In the second subsection, we show the Jacobian of

such global pose with respect to all the joints encodes the dependency information. Such dependencies from all sensors are concatenated as a binary matrix, we name it Heterogeneous Dependency Matrix. The third subsection discusses how such matrix can be learned by a data-driven method. In the fourth subsection, we go back to the robot's body, we show that a tree structure can be extracted from an open-chain robot, we call it Heterogeneous Out-tree. Subsection III-E shows the matrix and the out-tree are equivalent representations of the robot topology. We proposed two theorems to discuss the conditions when any binary matrix is a Heterogeneous Dependency Matrix. Subsection III-F discusses the case of partial observability that some links have no sensor mounted, while subsection III-H discusses another case when an erroneous matrix is extracted, how can it be fixed. The last subsection summarizes our method and shows how such a framework can be used to find robot body topology.

A. Exteroception Estimation

The first thing we need to find is the relation between proprioception and exteroception data in expressing the FK. Then the Jacobian of such FK can encode the dependency information. Assuming we have a second-order differentiable function approximator $f_\phi(\theta)$

$$f_\phi(\theta) = \mathbf{T}_\phi(\theta) = \begin{bmatrix} \mathbf{R}(\theta) & \mathbf{b}(\theta) \\ \mathbf{0} & 1 \end{bmatrix} = \begin{bmatrix} \mathbf{n}_x & \mathbf{n}_y & \mathbf{n}_z & \mathbf{b} \\ 0 & 0 & 0 & 1 \end{bmatrix} \quad (1)$$

which is parameterized by ϕ . The function approximator is used to map the input joint angle vector θ to a homogeneous transformation $\mathbf{T}_\phi(\theta) \in \mathbb{R}^{4 \times 4}$ in SE(3), that describes the transformation that sensor frame B described in global frame G . Reader should keep in mind that for each sensor on the robot body, there will be a unique $f_\phi(\theta)$ to represent the pose of the sensor, we only discuss one of them, and the rest are used in the same way. Due to lacking of the knowledge of the robot body structure, the ground-truth homogeneous transformation is unknown, that is why we use such an approximator to learn it from data. We denote the first and second-order derivative of $f_\phi(\theta)$ as $\frac{\partial f_\phi(\theta)}{\partial \theta} = \mathbf{J}_\phi(\theta) \in \mathbb{R}^{4 \times 4 \times N}$ and $\frac{\partial^2 f_\phi(\theta)}{\partial \theta^2} = \mathbf{H}_\phi(\theta) \in \mathbb{R}^{4 \times 4 \times N \times N}$, where N is the number of joints. We can also measure the proprioception as the angles, angular velocities and angular accelerations for all the joint angles (though we do not know their hierarchy) as $\theta, \dot{\theta}, \ddot{\theta}$. The exteroception data are the vectors $[\alpha_B, \beta_B]^T$ of linear acceleration and angular velocity (by roll-pitch-yaw) described in sensor frame, where $\alpha_B \in \mathbb{R}^3, \beta_B \in \mathbb{R}^3$. We will ignore the symbol of dependency of θ for all variables to make the result neat. The first and second-order time derivative of $f_\phi(\theta)$ are shown in Equations 2 and 3 as $\frac{\partial f_\phi}{\partial t} \in \mathbb{R}^{4 \times 4}$ and $\frac{\partial^2 f_\phi}{\partial t^2} \in \mathbb{R}^{4 \times 4}$.

$$\frac{\partial f_\phi}{\partial t} = \begin{bmatrix} \dot{\mathbf{R}} & \dot{\mathbf{b}} \\ \mathbf{0} & 1 \end{bmatrix} = \mathbf{J}_\phi \dot{\theta} \quad (2)$$

$$\frac{\partial^2 f_\phi}{\partial t^2} = \begin{bmatrix} \ddot{\mathbf{R}} & \ddot{\mathbf{b}} \\ \mathbf{0} & 1 \end{bmatrix} = \mathbf{H}_\phi \ddot{\theta} + \mathbf{J}_\phi \ddot{\theta} \quad (3)$$

The two equations show that we can estimate $\dot{\mathbf{R}}, \dot{\mathbf{b}}, \ddot{\mathbf{R}}$ and $\ddot{\mathbf{b}}$ by exteroception and proprioception data. The next step is to find the relation between $\mathbf{R}, \mathbf{b}, \dot{\mathbf{R}}, \dot{\mathbf{b}}, \ddot{\mathbf{R}}, \ddot{\mathbf{b}}$ and $[\alpha_B, \beta_B]^T$.

For any point r in space, we have

$$r_G = \mathbf{T}_\phi \cdot r_B \quad (4)$$

r_G and r_B are coordinates of the same r in global and sensor frame respectively. By taking the second-order time derivative of such relation, we have the acceleration of point r in sensor frame:

$$a_B = \mathbf{T}_\phi^{-1} a_G = \mathbf{T}_\phi^{-1} \ddot{r}_G = \mathbf{T}_\phi^{-1} \cdot \ddot{\mathbf{T}}_\phi \cdot r_B = \begin{bmatrix} \mathbf{R}^T \ddot{\mathbf{R}} & \mathbf{R}^T \ddot{\mathbf{b}} \\ \mathbf{0} & \mathbf{0} \end{bmatrix} \cdot r_B \quad (5)$$

We conclude that the linear part α_B equals $\mathbf{R}^T \ddot{\mathbf{b}}$ because they are both in \mathbb{R}^3 . Then we need to find the angular part. Define operation

$$\omega_B^\wedge = \begin{bmatrix} w_1 \\ w_2 \\ w_3 \end{bmatrix}^\wedge = \begin{bmatrix} 0 & -w_3 & w_2 \\ w_3 & 0 & -w_1 \\ -w_2 & w_1 & 0 \end{bmatrix} \quad (6)$$

To find the expression of β_B , we already know the expression of angular velocity in body frame, as $\omega_B^\wedge = \mathbf{R}^T \dot{\mathbf{R}}$. However, the corresponding vector ω_B is not β_B because ω_B is the rotation velocity vector described by axis-angle system and β_B is the rotation velocity vector described by roll-pitch-yaw system. To align the two representations, we know the two velocity vectors should cause the same rotation effect in a short period of time T_s . For ω_B , it can be decomposed to a time derivative of an angle $\dot{\vartheta} \in \mathbb{R}$ and a rotation axis vector $\vec{u} \in \mathbb{R}^3$, with $\omega_B = \dot{\vartheta} \vec{u}$ and $|\vec{u}| = 1$. The rotated angle in T_s can be approximated as $\dot{\vartheta} T_s$. By Rodrigues' rotation formula, the corresponding rotation matrix in T_s is

$$\mathbf{R}_1 = \mathbf{I} + \sin(\dot{\vartheta} T_s) \omega_B^\wedge + [1 - \cos(\dot{\vartheta} T_s)] \omega_B^\wedge \cdot \omega_B^\wedge \quad (7)$$

For β_B , it represents the roll, pitch, yaw velocities as $\beta_B = [\beta_{B1}, \beta_{B2}, \beta_{B3}]^T$. The rotated angle in T_s can be approximated by $[\beta_{B1} \cdot T_s, \beta_{B2} \cdot T_s, \beta_{B3} \cdot T_s]^T$, so the rotation matrix can be calculated from standard roll-pitch-yaw rotation matrices as

$$\mathbf{R}_2 = \mathbf{R}_z(\beta_{B3} \cdot T_s) \mathbf{R}_y(\beta_{B2} \cdot T_s) \mathbf{R}_x(\beta_{B1} \cdot T_s) \quad (8)$$

\mathbf{R}_z , \mathbf{R}_y and \mathbf{R}_x are rotation matrices w.r.t. z, y and x axes. For who is not familiar with the context, one can refer to Appendix A for a more detailed derivation. Apparently \mathbf{R}_1 and \mathbf{R}_2 should be the same matrix because they express the same rotation effect in T_s . As \mathbf{R}_1 is proposed from $f_\phi(\theta)$ and \mathbf{R}_2 is calculated from measurement β_B , we can learn the parameter ϕ by minimizing their difference. For any rotation matrix \mathbf{R} , we have $\text{tr}(\mathbf{R}) = 1 + 2\cos(\rho)$, ρ is the angle of rotation described in angle-axis system, so

$$\rho = \arccos \frac{\text{tr} \mathbf{R} - 1}{2} \quad (9)$$

In our case, matrix \mathbf{R} is the relative rotation between \mathbf{R}_1 and \mathbf{R}_2 which is $\mathbf{R} = \mathbf{R}_1^T \mathbf{R}_2$. When the two matrices are the same, we have $\rho = 0$.

Thus, we can find the optimal parameter ϕ^* by

$$\phi^* = \underset{\phi}{\text{argmin}} \left[\left| \alpha_B - \mathbf{R}^T \ddot{\mathbf{b}} \right| + \arccos \frac{\text{tr}(\mathbf{R}_1^T \mathbf{R}_2) - 1}{2} \right] \quad (10)$$

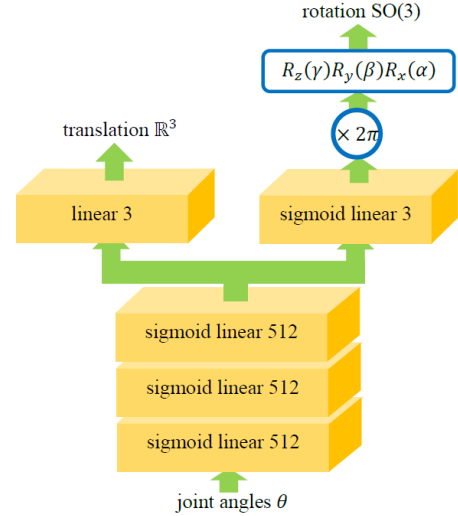


Fig. 2: Neural network structure of $f_\phi(\theta)$. The roll-pitch-yaw angles to rotation matrix transformation can be found in Equation 12. The result will be reshaped to a homogeneous transformation matrix of 4×4 by padding zeros and ones as Equation 1.

Using gradient descent method can potentially cause some numerical problem by arccos term. In practice, we found using the following optimization can also have good performance.

$$\phi^* = \underset{\phi}{\text{argmin}} \left[\left| \alpha_B - \mathbf{R}^T \ddot{\mathbf{b}} \right| - \text{tr}(\mathbf{R}_1^T \mathbf{R}_2) \right] \quad (11)$$

The detailed derivation of this section can be seen in Appendix A.

In our work, we use a neural network to represent $f_\phi(\theta)$, whose structure is shown in Figure 2. The input of the neural network is the joint angle vector of \mathbb{R}^n . Through three hidden layers with sigmoid activation function, the translation branch consists of 3 linear neurons predicting global translation in \mathbb{R}^3 . The rotation branch consists of 3 linear neurons predicting the roll-pitch-yaw angles $[\alpha, \beta, \gamma]^T$ in $[0, 2\pi]$. Such angles will be transformed to a rotation matrix with

$$\mathbf{R}_2 = \mathbf{R}_z(\gamma) \mathbf{R}_y(\beta) \mathbf{R}_x(\alpha) \quad (12)$$

The rotation part and translation part of the neural network output will be concatenated as a homogeneous transformation matrix as shown in Equation 1. Notice that for each exteroception sensor (IMU), there will be a unique neural network attached to it (shown in Figure 3 left). It means if there is 1000 sensors, there will be 1000 such networks trained in parallel. It also indicates the system is linearly scalable with the increasing of number of sensors.

B. Heterogeneous Dependency Matrix

In last subsection, we have already learned a proposed homogeneous transformation $\mathbf{T} = f_\phi(\theta)$ to approximate the global pose of the sensor linked with it. However, as we have not specified the reference frame, the value of such homogeneous transformation can be arbitrary. We can assume the

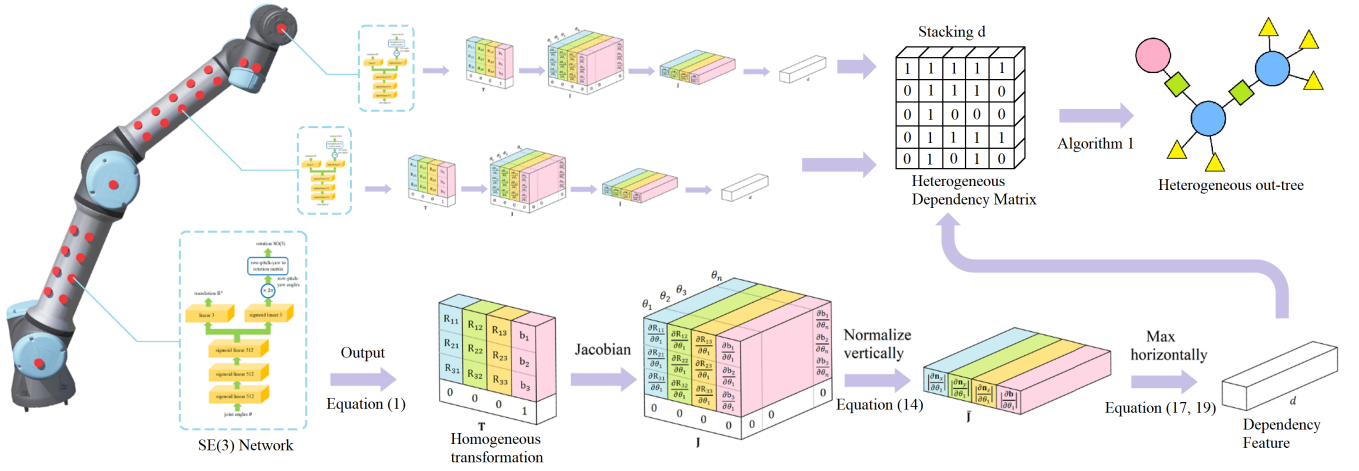


Fig. 3: Pipeline to extract robot body structure (represented by a heterogeneous out-tree). (left) Each IMU is linked to a SE(3) neural network as shown in Figure 2 to approximate its global pose given the joint angles. (bottom) each neural network $f_\phi(\theta)$ outputs the current homogeneous transformation \mathbf{T} ; The 'Jacobian' step extracts Jacobian matrix \mathbf{J} of size $(4, 4, N)$ from \mathbf{T} ; normalize by each column to get Transform Invariant Jacobian $\bar{\mathbf{J}}$; extract Dependency Feature \mathbf{d} from $\bar{\mathbf{J}}$ by Equation 15. (right) stack all Dependency Features from all sensors and merge the duplicates generates a heterogeneous dependency matrix; running algorithm 1 to generate the out-tree from the matrix.

Jacobian of $f_\phi(\theta)$ can encode the true dependency information of how the change of each joint angle affects the change of output, but it is also reference frame dependent. However, when \mathbf{T} is irrelevant to some joint value θ , the corresponding term in Jacobian matrix should be zero, and that is reference frame independent. In this section, we show a way to extract the reference frame independent Jacobian representation. The concatenation of such representations from all sensor frames can form a new matrix, which records the global dependency information.

Definition 1. If we have homogeneous transformation \mathbf{T} as defined in Equation 1, the homogeneous Jacobian w.r.t configuration θ can be represented as a $12 \times N$ matrix as:

$$\frac{\partial \mathbf{T}}{\partial \theta} = \left[\frac{\partial \mathbf{n}_x}{\partial \theta}, \frac{\partial \mathbf{n}_y}{\partial \theta}, \frac{\partial \mathbf{n}_z}{\partial \theta}, \frac{\partial \mathbf{b}}{\partial \theta} \right]^T \quad (13)$$

The Transform Invariant Jacobian is defined as a $4 \times N$ matrix as:

$$\bar{\mathbf{J}} = \left[\left| \frac{\partial \mathbf{n}_x}{\partial \theta} \right|, \left| \frac{\partial \mathbf{n}_y}{\partial \theta} \right|, \left| \frac{\partial \mathbf{n}_z}{\partial \theta} \right|, \left| \frac{\partial \mathbf{b}}{\partial \theta} \right| \right]^T \quad (14)$$

$|\cdot|$ is to normalize by each column. N is the number of joints.

We show (in Appendix B) that $\bar{\mathbf{J}}$ is invariant to the choice of the reference frame, which means no matter where the sensor is mounted, as long as it is mounted on the same link, such Jacobian should keep the same.

Proposition 1. Transform Invariant Jacobian is invariant to any joint-independent transformation $\mathbf{Y} \in SE(3)$.

As Jacobian encodes the dependency of change of pose with respect to joints, we assume it to be a feature of sensor dependency that carries topology information. We can

transform such feature into a more concise representation. The idea is we only care about if a frame i has dependency on joint θ_j or not. In such case, we can turn Transform Invariant Jacobian to a binary representation.

Definition 2. There is one corresponding Dependency Feature $\mathbf{d} \in \mathbb{R}^N$ to each Transform Invariant Jacobian $\bar{\mathbf{J}}$. Dependency Feature is defined as $\mathbf{d}_n = 0$ if all the elements in n -th column of $\bar{\mathbf{J}}$ are zeros. Else $\mathbf{d}_n = 1$.

For example,

$$\bar{\mathbf{J}} = \begin{bmatrix} 3.14 & 6.23 & 0 & 1.56 \\ 7.23 & 2.64 & 0 & 3.25 \\ 2.33 & 3.08 & 0 & 6.32 \\ 7.33 & 8.32 & 0 & 9.17 \end{bmatrix} \rightarrow \mathbf{d} = [1, 1, 0, 1] \quad (15)$$

Notice that each column of \mathbf{d} has a unique label θ_j . The "1" positions in Dependency Feature encodes all the joints that the sensor frame passes as it traverses to the root. The pipeline to extract Dependency Feature is shown in Figure 3 bottom.

Definition 3. Heterogeneous Dependency Matrix \mathbf{D} is defined as stacking Dependency Feature \mathbf{d} of all the sensors (not on root node) as rows in a matrix, with duplicate rows merged (only one left).

The Dependency Feature stacking is shown in Figure 3 right, forming a Heterogeneous Dependency Matrix. The duplicate rows in such matrix are introduced by two sensors mounted on the same link, which we know from proposition 1. Dependency features of different sensors on the same link are identical because the sensors traverse the same set of joints to the root. Merging the duplicate rows ensures the redundant dependency information is eliminated.

Heterogeneous dependency matrix is a labelled matrix. In our case, the row labels are different sensors and the column

$$\begin{array}{ccc} & d & e & f \\ a & \begin{bmatrix} 1 & 1 & 0 \end{bmatrix} \\ b & \begin{bmatrix} 0 & 1 & 1 \end{bmatrix} \\ c & \begin{bmatrix} 0 & 1 & 0 \end{bmatrix} \end{array} \quad \begin{array}{ccc} & e & d & f \\ a & \begin{bmatrix} 1 & 1 & 0 \end{bmatrix} \\ c & \begin{bmatrix} 1 & 0 & 0 \end{bmatrix} \\ b & \begin{bmatrix} 1 & 0 & 1 \end{bmatrix} \end{array}$$

Fig. 4: Two matrices transformed by switching rows [b,c] and columns [d,f]; we assume they are equivalent.

labels are different joints. We also have to ensure each entity of sensors and joints are physically distinguishable (apparent in our case because they are measured).

Property 1. Rows and columns of \mathbf{D} are interchangeable.

Property 2. Rows and columns of \mathbf{D} are non-duplicate.

Property 1 is obvious because rows are labels of sensors without order. For columns, because each row is a Dependency Feature records the binary dependency of joint nodes on the route from the sensor to the root, this dependency is agnostic to the order of joints. Notice that interchanging rows and columns of \mathbf{D} is accompanied by interchanging their labels. Because the rows and columns of \mathbf{D} are labelled, we assume any permutation of rows and columns represents the same matrix (Figure 4). Property 2 is shown in Appendix C.

C. Data-driven Remedy

Before we continue to the next section, we need to solve some problems when we learn and extract heterogeneous dependency matrix by the data-driven method. The first problem we are faced with is that the Transform Invariant Jacobian is actually a function of θ . However, what we need is a real number matrix as in Example 15. Here comes a question that which value of θ we choose to calculate such matrix. Here, we independently sampled θ s, e.g., from a random joint motion or uniformly sample in configuration space and then calculate the variance of their corresponding Jacobians.

$$\begin{aligned} \bar{\mathbf{J}} &= \mathbb{E}_{\theta} \left[\left(\bar{\mathbf{J}}_{\phi}(\theta) - \mathbb{E}_{\theta} [\bar{\mathbf{J}}_{\phi}(\theta)] \right)^2 \right] \\ &= \frac{1}{n} \sum_{i=1}^n \left[\bar{\mathbf{J}}_{\phi}(\theta_i) - \frac{1}{n} \sum_{i=1}^n \bar{\mathbf{J}}_{\phi}(\theta_i) \right]^2 \end{aligned}$$

We can also use mean or median value, but we found using variance provides the most stable result. The idea behind this is when sensor i 's movement is independent of joint j , the j 's column of $\bar{\mathbf{J}}$ should be all-zero, no matter what θ is. Thus, the variance of such column must also be zero. Otherwise, there must be some θ s that cause the j 's column of $\bar{\mathbf{J}}$ non-zero, then the variance is also non-zero. So, variance also retains the dependency information that Jacobian carries.

Then, we should discuss the problem of Jacobian \mathbf{J}_{ϕ} and its underlying function approximator f_{ϕ} . In ideal case, $f_{\phi}(\theta)$ perfectly catches the FK and the Transform Invariant Jacobian $\bar{\mathbf{J}}$ is noiseless. However noise could be naturally brought by data that the all-0 columns in $\bar{\mathbf{J}}$ will not be zero (as in Example 15), or duplicate rows can be non-duplicate, which means Heterogeneous Dependency Matrix can have more rows than columns.

For the first problem, we can filter $\bar{\mathbf{J}}$ by a max function instead of Example 15 and normalize such feature.

$$\mathbf{d}' = \max_{row} \bar{\mathbf{J}} / \left| \max_{row} \bar{\mathbf{J}} \right| \quad (16)$$

For example,

$$\begin{aligned} \bar{\mathbf{J}} &= \begin{bmatrix} 3.14 & 6.23 & 0 & 1.56 \\ 7.23 & 2.64 & 0 & 3.25 \\ 2.33 & 3.08 & 0 & 6.32 \\ 7.33 & 8.32 & 0 & 9.17 \end{bmatrix} \rightarrow \mathbf{d}' = [7.33, 8.32, 0, 9.17] \\ &\rightarrow \mathbf{d}' = [0.5, 0.57, 0, 0.63] \end{aligned} \quad (17)$$

Then we can use a threshold function to get \mathbf{d} as

$$\mathbf{d}_i = \begin{cases} 1 & \text{if } \mathbf{d}'_i > \delta \\ 0 & \text{otherwise} \end{cases} \quad (18)$$

For the second problem (more rows than columns), we can use Dirichlet Process Gaussian Mixture Model (DPGMM [23]) to cluster all rows \mathbf{d} , and sample rows (no more than the number of columns) from the DPGMM. Notice the sampled rows are not binary vectors, we have to filter them with a threshold of 0.5 (because the rows in each cluster are all binary). Then the sampled rows form a new Heterogeneous Dependency Matrix.

A new problem is introduced that what is the optimal value of threshold δ ? The criterion of choosing δ is that δ should ensure among clusters more separated and in each cluster less dispersed. Also, it should ensure the numbers of samples in different clusters are similar. We propose to optimize δ as

$$\begin{aligned} \mathbf{S}_{i,j} &= |\mu_i - \mu_j| \\ m &= \sum_{\forall c} \sum_{x_i \in c} (x_i - \mu_c)^T (x_i - \mu_c) \\ p_c &= \frac{n_c}{\sum_c n_c} \\ \delta^* &= \arg\max_{\delta} \frac{\det(\mathbf{S})}{m} - \lambda \sum_c p_c \cdot \log(p_c) \end{aligned} \quad (19)$$

λ is a weighting factor. Here, matrix \mathbf{S} stores the distance information between means of any two clusters. m captures the dispersion of data in each cluster by summing up the dispersion in each cluster. p_c is the number of data points in cluster c based on the total number of data points. The optimal δ^* maximizes \mathbf{S} to separate clusters, minimizes m to reduce data dispersion in each cluster, and maximizes the entropy of p_c to make numbers of samples in different clusters similar.

D. Heterogeneous Out-tree

In the previous section, we discussed how to extract heterogeneous dependency matrix \mathbf{D} from data, we aim to find the relation between \mathbf{D} and the robot forward kinematics (body structure). For an open-chain robot with sensors mounted on the body links, we can have its body representation as in Figure 5a. We can easily find each dependency feature actually encodes all the joint nodes on the route from the sensor to the root. If we merge all the same rows, the equivalent robot structure is that there is exactly one sensor on each link. In

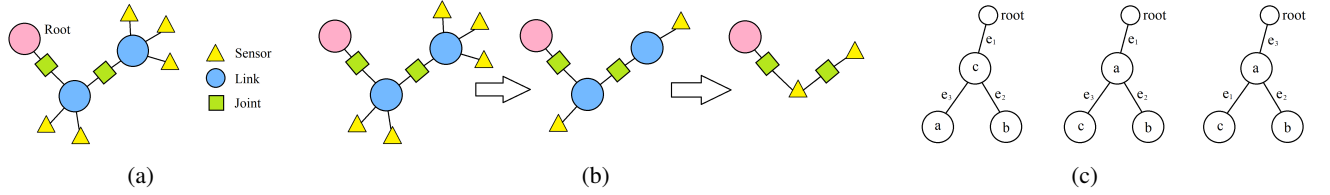


Fig. 5: (a) Topology of open-chain robot. (b) Topology simplification of a robot. The first arrow is because different sensors on the same link provide redundant joint-dependency information. The second arrow is because link and sensor are one-one pair, so it is equivalent to discuss either. (c) Examples of heterogeneous out-tree.

such case, the sensors and links are one-one pair and rigidly mounted, so they will share the same dependency. Then we do not need to discuss three different types of nodes in such topology, but only two types are enough (joints and sensors). Such simplification is shown in Figure 5b. We keep the sensor nodes in the final tree structure because they are directly observable, but not for link nodes. Notice such tree has a direction from root to all leaf nodes but is not shown in the figure. Also, every sensor node or joint node is unique (reader can imagine they are labelled), which means if any two nodes switch, then it results in a different tree. We can also assume sensors are nodes and joints are edges.

Definition 4. Heterogeneous Out-Tree is defined as an out-tree with all edges labelled.

Different from out-trees, heterogeneous out-tree not only considers the parent of each node, but also considers via which particular edge, the node inherits from its parent. Figure 5c shows some heterogeneous out-trees with nodes $[a, b, c, \dots]$ and edges $[e_1, e_2, e_3, \dots]$, they are different trees.

Definition 5. Two heterogeneous out-trees are semi-equivalent if any node with the same label in both trees has the same parent node.

Semi-equivalent tree neglects the dependency for nodes of edges. For example, tree 2 and tree 3 in Figure 5c are semi-equivalent but not equivalent.

Property 3. In a heterogeneous out-tree, the number of nodes is $N + 1$ and the number of edges is N .

Property 4. $\sum_j D_{ij}$ is the depth of node i in the tree.

Property 5. There are $(N + 1)^{N-1} \cdot N!$ different tree structures with N nodes.

Property 5 is proved in Appendix D. The following lemma (proof in Appendix E) links such an out-tree with heterogeneous dependency matrix introduced in section III-B.

Lemma 1. From each heterogeneous out-tree, one can extract a determined heterogeneous dependency matrix.

We define the set of all possible topologies of heterogeneous out-tree consisting of N nodes as \mathbb{T}_N .

Definition 6. We define two operations on set \mathbb{T}_N . For any heterogeneous out-tree $t \in \mathbb{T}_N$:

Dilation: Given a node i whose direct parent node is root, direct parent edge e_i , and given another node j , the dilation

operation $di^{i \rightarrow j}(t)$ moves e_i to the direct child edge of j .

Absorption: Given a leaf node i , and direct parent edge is e_i whose direct parent node is j (non-root), the absorption operation $ab^{j \rightarrow i}(t)$ moves e_i to the direct child edge of root.

Figure 6a illustrates an example of dilation and absorption. The following properties are proved in Appendices F-H.

Lemma 2. $ab^{j \rightarrow i}(t)$ and $di^{i \rightarrow j}(t)$ on heterogeneous out-tree set are a pair of inverse operation.

Proposition 2. Any tree t can be transformed to a depth-1 tree by a series of absorption and from the depth-1 tree, reconstruct the original tree t .

Corollary 1. Tree set \mathbb{T}_N is closed under dilation and absorption.

In the following sections, we will shown how the heterogeneous dependency matrix and heterogeneous out-tree are related.

E. Tree-Matrix Equivalence

We now discover if heterogeneous dependency matrix and heterogeneous out-tree have some shared properties. We define the set of all binary matrices $\{0, 1\}^{N \times N}$ as \mathbb{S}_N . Clearly, the matrices with corresponding heterogeneous out-trees consist of only a subset of \mathbb{S}_N . For example matrix

$$\begin{bmatrix} 1 & 1 & 0 \\ 0 & 1 & 1 \\ 1 & 0 & 1 \end{bmatrix} \quad (20)$$

has no corresponding heterogeneous out-tree. We define set of all binary matrices of $N \times N$ having corresponding heterogeneous out-trees as \mathbb{D}_N . $\mathbb{D}_N \subseteq \mathbb{S}_N$.

Definition 7. We define two operations on set \mathbb{S}_N . For any matrix $\mathbf{S} \in \mathbb{S}_N$:

Absorption: For any row i and j , $i \neq j$, perform an XOR operation, $\mathbf{s}' = \mathbf{S}_i \oplus \mathbf{S}_j$. If $\sum \mathbf{s}' = 1$ and $\sum \mathbf{S}_i > \sum \mathbf{S}_j$, absorption $ab^{j \rightarrow i}(\mathbf{S})$ makes $\mathbf{S}_i := (\mathbf{S}_i - \mathbf{S}_j) \bmod 2$; otherwise, do nothing.

Dilation: For any row i and j , $i \neq j$, if $\sum \mathbf{S}_i = 1$ and $\mathbf{S}_i \cap \mathbf{S}_j = 0$, dilation $di^{i \rightarrow j}(\mathbf{S})$ makes $\mathbf{S}_i := (\mathbf{S}_i + \mathbf{S}_j) \bmod 2$; else, do nothing.

In other words, if \mathbf{S}_i inherits all “1”s in \mathbf{S}_j and has one more “1” than \mathbf{S}_j , absorption makes \mathbf{S}_i get rid of “1”s that \mathbf{S}_i and \mathbf{S}_j have in common and only leaves the “1” that \mathbf{S}_i has

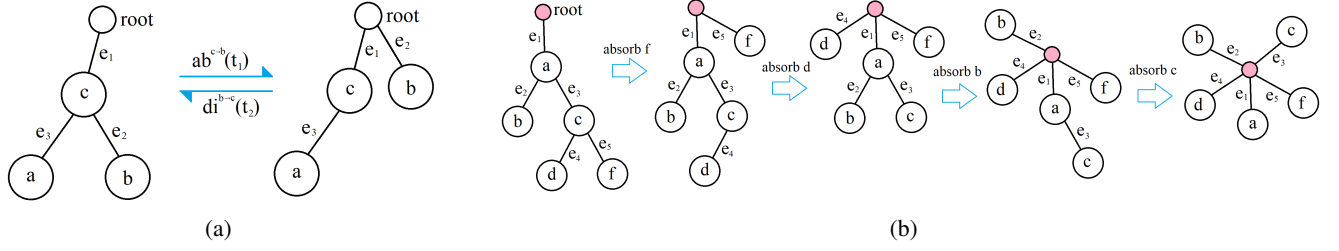


Fig. 6: (a) Demonstration of dilation $di^{i \rightarrow j}(t)$ and absorption $ab^{j \rightarrow i}(t)$. (b) Demonstration of using absorption operation to transform a tree to a depth-1 tree.

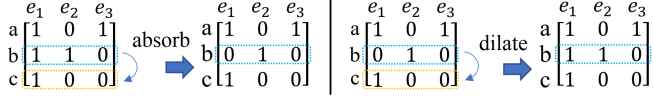


Fig. 7: Absorption and dilation on matrix set. Matrices correspond to trees in Figure 6a.

$$\begin{bmatrix} d & e & f \\ a & 1 & 0 & 0 \\ b & 0 & 1 & 0 \\ c & 0 & 0 & 1 \end{bmatrix} \neq \begin{bmatrix} d & f & e \\ a & 1 & 0 & 0 \\ b & 0 & 1 & 0 \\ c & 0 & 0 & 1 \end{bmatrix}$$

Fig. 8: Different permutation matrices

but S_j not. Dilation can work only when S_i and S_j shares no common “1”s and there is only one “1” in S_i . An example performing dilation and absorption is shown in Figure 17. The following tree-matrix equivalence holds (proof in Appendix I):

Proposition 3. For any heterogeneous out-tree $t \in \mathbb{T}_N$ and its generated heterogeneous dependency matrix $\mathbf{D} \in \mathbb{D}_N$, absorption operation on t is equivalent to absorption operation on \mathbf{D} . Similarly, this is true for dilation.

Proposition 4. The tree to matrix translation in Lemma 1 is bijective.

From proposition 4 (proved in Appendix J), we know heterogeneous dependency matrix is a complete representation of heterogeneous out-tree; we interchange both names in later sections. In the previous section, we only consider \mathbf{D} generated from a tree, but without discussing what properties \mathbf{D} should have. The following theorem tells us under what condition a binary matrix is a heterogeneous dependency matrix.

Theorem 1. For any binary matrix $\mathbf{D} \in \{0,1\}^{N \times N}$, it has unique corresponding heterogeneous out-tree iff it can be transformed to an permutation matrix \mathbf{I} by a sequence of absorption and dilation.

The proof is in Appendix K. The theorem 1 does not imply that all trees can be reduced to the same permutation matrix. As the heterogeneous dependency matrices are labelled, permutation matrices in Figure 8 are different instances.

We now show more properties of \mathbf{D} .

Definition 8. For a column c , its Column set S_c is defined as the set of rows that intersect column c . $S_c =$

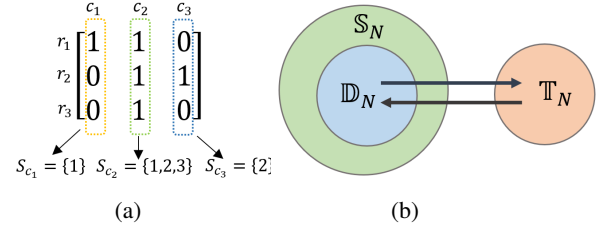


Fig. 9: (a) Column set example. (b) Relation among heterogeneous dependency matrix set \mathbb{D}_N , heterogeneous out-tree set \mathbb{T}_N and binary matrix set \mathbb{S}_N .

$$\{r \in \text{row}(\mathbf{D}) \mid \mathbf{D}_{(r,c)} = 1\}.$$

Each column has its own column set, which is the collection of the corresponding row labels that the elements in the column is 1, as shown in Figure 9a. It represents all the nodes in the sub-tree rooted in column c .

Definition 9. Define J_{S_c} the Unique Element Set of S_c , if $J_{S_c} = S_c \setminus \bigcup_{c' \in \text{col}(\mathbf{D}): S_{c'} \subsetneq S_c} S_{c'}$.

J_{S_c} is the set of $r \in \text{row}(\mathbf{D})$ such that r is in S_c but not in any $S_{c'}$ which is a proper subset of S_c . For example in Figure 9a, $J_{S_{c_1}} = \{1\}$, $J_{S_{c_3}} = \{2\}$, because S_{c_1} and S_{c_3} has no proper subset. S_{c_1} and S_{c_3} are the proper subsets of S_{c_2} , so $J_{S_{c_2}}$ should only include row labels that only appear in S_{c_2} but not in S_{c_1} or S_{c_3} , which is $J_{S_{c_2}} = \{3\}$.

Definition 10. Consider the following conditions for \mathbf{D} :

- 1) There are no all-0 rows in \mathbf{D} .
- 2) There are no all-0 columns in \mathbf{D} .
- 3) There are no duplicate rows in \mathbf{D} .
- 4) There are no duplicate columns in \mathbf{D} .
- 5) $\forall c_1, c_2 \in \text{col}(\mathbf{D}), S_{c_1} \subseteq S_{c_2}$ or $S_{c_1} \supseteq S_{c_2}$ or $S_{c_1} \cap S_{c_2} = \emptyset$
- 6) $\forall c, |J_{S_c}| = 1$

We also define some sets of conditions:

$$P = \{1^\circ, 2^\circ, 3^\circ, 4^\circ, 5^\circ\} \quad P_0 = \{1^\circ, 2^\circ, 5^\circ, 6^\circ\}$$

We denote a matrix \mathbf{D} subject to a set of conditions P as $\mathbf{D} : P$

Proposition 5. A matrix $\mathbf{D} \in \{0,1\}^{n \times n}$ satisfies $P_0 \Leftrightarrow \mathbf{D}$ satisfies P .

Theorem 2. A matrix \mathbf{D} satisfies P is equivalent to matrix \mathbf{D} can be translated to a heterogeneous out-tree.

Proofs can be found in Appendix L and N. Proposition 5 tells us condition sets P and P_0 are equivalent, $\mathbf{D} : P \Leftrightarrow \mathbf{D} : P_0$. Theorem 2 then shows that such \mathbf{D} under condition set P (or P_0) is equivalent to a heterogeneous out-tree. If a binary matrix fulfills condition set P , it is a heterogeneous dependency matrix, and can be grown to a heterogeneous out-tree. We propose an algorithm to do the matrix to out-tree translation, as shown in Algorithm 1. Such translation can be found in pipeline Figure 3 right, where a heterogeneous out-tree is output at the final stage of our system. A demonstration of running the algorithm translating an example matrix to an out-tree is in Appendix M.

Algorithm 1: Matrix to Out-tree Translation Algorithm

Input: row set $\mathbf{r} = \{r_i\}$ in \mathbf{D} , root node, explored set $E = \emptyset$.
while $\mathbf{r} \neq \emptyset$ **do**
 find r_{min} in \mathbf{r} with minimal depth.
 pop r_{min} from \mathbf{r}
 if depth of r_{min} is 1 **then**
 The column label with the "1" entry is e . Attach r_{min} to root by edge e .
 else
 find one r' in E that $r_{min} - r' = 1$. The column label with the "1" entry is e . Attach r_{min} to r' by edge e .
 end if
 push r_{min} in E .
end while
Output: heterogeneous out-tree from root node

The core idea of this section is shown in Figure 9b. Proposition 4 shows that the bi-directional arrows hold, the out-tree set \mathbb{T}_N and matrix set \mathbb{D}_N are different representations of the same thing. Theorem 1 and 2 tells us when any binary matrix in \mathbb{S}_N is a heterogeneous dependency matrix in \mathbb{D}_N . They are proven from different perspectives.

F. Partial Observability

In this section, we will discuss the partial observability problem. In the ideal case, each link will have some sensors mounted on, so that the sensors and links are one-one pair as Figure 5b shows. The heterogeneous dependency matrix is a square matrix of $N \times N$. However, when there are some links with no sensor mounted on, the movement or the dependency of such link is unobservable. The heterogeneous dependency matrix will have fewer rows than columns. If we need to extract a valid heterogeneous out-tree, we need to complete such matrix to square and also ensure it follows condition in theorem 1 or 2. In this section, we will discuss under what condition the matrix can be completed to a square matrix and how such completion can be performed.

Let \mathbf{D}^- be a sub-matrix of $\mathbf{D} : P$ of size $K * N$, where $K < N$. We now consider if such \mathbf{D}^- has a corresponding tree. The first problem is whether we can fill \mathbf{D}^- to a \mathbf{D} of

size $N \times N$, that is to get rid of partial observability. Because multiple different \mathbf{D} can be cut to the same sub-matrix \mathbf{D}^- , we assume such filling may not be unique. Notice that we are discussing general \mathbf{D}^- and \mathbf{D} , not necessarily compliant to any constraint set P . The following theorem shows when such filling exists and when the filling is unique. We define another set of condition $P^- = \{1^\circ, 3^\circ, 5^\circ\}$.

Theorem 3. A $\mathbf{D}^- : P^-$ can be filled to a $\mathbf{D} : P$. Such filling is unique when $N - K = 1$ and there is one J_{S_c} is \emptyset .

Proof can be found in Appendix P. Theorem 3 tells us, a \mathbf{D}^- can be filled to $\mathbf{D} : P$ if and only if $\mathbf{D}^- : P^-$. The filling is not unique unless $N - K = 1$ and there is one J_{S_c} is \emptyset . In that case, there will be a unique corresponding tree and the topology of the robot is fully determined.

G. Matrix Completion Algorithm

Knowing the conditions that a \mathbf{D}^- can be filled to a \mathbf{D} is not enough. We need to design a Matrix Completion Algorithm (Algorithm 2) to perform such filling. We proposed an algorithm to fill \mathbf{D} from \mathbf{D}^- if \mathbf{D}^- fulfills condition set P^- , as is shown in Algorithm 2. We showed an example running such algorithm to fill \mathbf{D}^- in Appendix O.

Algorithm 2: Matrix Completion Algorithm

Input: partial matrix \mathbf{D}^- of $K \times N$.
 Calculate S_c and J_{S_c} for each column c in \mathbf{D}^- .
 Randomly pick K different columns with different J_{S_c} , and push the rest columns' labels (edge) in set $a = \emptyset$.
 Push the $N - K$ unobserved rows' labels (nodes) in set $b = \emptyset$.
 while $a \neq \emptyset$ **do**
 Pull one edge c from a and one node v from b .
 Add a new row to \mathbf{D}^- .
 for all columns c' in \mathbf{D}^- **do**
 if $S_c \subseteq S_{c'}$ **then**
 Set $\mathbf{D}_{v,c'}^- = 1$
 end if
 end for
 end while
Output: Complete matrix \mathbf{D} .

H. Contradiction

In this section, we discuss matrices that do not follow Theorem 1 or Theorem 2. Such violation will not happen if such matrix is directly extracted from a heterogeneous tree. However, if such matrix is learned from some noisy observations or data-driven methods, the extracted matrix can be erroneous. For example, matrix

$$\begin{bmatrix} 1 & 1 & 0 \\ 0 & 1 & 1 \\ 1 & 0 & 1 \end{bmatrix} \quad (21)$$

does not have any corresponding heterogeneous out-tree (certainly, it also does not follow theorem 1 and 2). We still need

to infer the tree structure by finding the most similar matrix $\mathbf{D} \in \mathbb{D}_N$ to it which encodes the most possible tree structure. The most straightforward way is to enumerate all possible tree structures spanned by N nodes and edges, compare each one with the erroneous matrix, and choose the one with minimal difference (e.g. Hamming distance). However due to Property 5, the enumerating will lead to an astronomical number when N grows. So an algorithm efficiently recovers the correct matrix is needed.

Inspired by Proposition 2, we know each tree corresponds to a depth-1 tree, or by Theorem 1, a permutation matrix. Such permutation matrices (Figure 8) encode the pairing of nodes and edges. Dilation or absorption on such permutation matrix will change the tree's topology but not such pairing. Thus, \mathbb{D}_N can be segmented by such $N!$ (pairing N edges with N nodes) different permutation matrices, each of them can grow to a class of trees that have different topology but the same nodes-edges pairing. Notice the "1"s in the permutation matrix should also appear in the matrix of the tree it grows to. So we can first find the most similar permutation matrix of the erroneous matrix, and from such permutation matrix to grow the most similar tree.

Algorithm 3: Matrix Correction Algorithm

Input: Erroneous matrix \mathbf{D} of $N \times N$.

Calculate the most similar permutation matrix \mathbf{I} by MILP as Equation 22.

$b = \{\mathbf{I}\}$, $g = +\infty$.

while true **do**

$b_{set} = \emptyset$, $d_{set} = \emptyset$

for each \mathbf{M} in b **do**

for $i, j \in N, i \neq j$ **do**

$\tilde{\mathbf{M}} = d_{i \rightarrow j}(\mathbf{M})$

$d_{\tilde{\mathbf{M}}} = \text{Hamming distance between } \tilde{\mathbf{M}} \text{ and } \mathbf{D}$.

$b_{set} = d_{set} \cup \tilde{\mathbf{M}}$, $d_{set} = d_{set} \cup d_{\tilde{\mathbf{M}}}$

end for

end for

$\tilde{g} = \min(d_{set})$

if $\tilde{g} = g$ **then**

 break

else

$g := \tilde{g}$, $b := b_{set}$ whose ones have $d_{\tilde{\mathbf{M}}} = \tilde{g}$

end if

end while

Output: Correct matrix candidates b .

Finding the most similar permutation matrix can be solved by enumerating all possible permutation matrices and comparing the overlapping. However, there are still $N!$ possible permutation matrices and will be less efficient when N grows. We turn such problem into a mixed-integer linear programming (MILP) problem. Though MILP is NP-Hard, in practice, we found it is very fast in finding the permutation matrix.

Let \mathbf{I} be the permutation matrix we want to find. We know that the original matrix \mathbf{D} and \mathbf{I} must share the positions where the "1"s are in \mathbf{I} . We represent such overlapping by another matrix $\mathbf{W}_{ij} = \min(\mathbf{D}_{ij}, \mathbf{I}_{ij})$. That means only when both

\mathbf{D}_{ij} and \mathbf{I}_{ij} are "1", \mathbf{W}_{ij} becomes "1" (overlapping). The optimization target becomes maximizing the total number of overlapping, which is:

$$\begin{aligned} & \max_{\mathbf{I}_{ij}, \mathbf{W}_{ij}} \sum_{i,j} \mathbf{W}_{ij} \\ \text{s.t. } & \sum_i \mathbf{I}_{ij} = 1, \quad \sum_j \mathbf{I}_{ij} = 1, \quad \mathbf{I}_{ij} \in \{0, 1\}, \\ & \mathbf{W}_{ij} \leq \mathbf{I}_{ij}, \quad \mathbf{W}_{ij} \leq \mathbf{D}_{ij} \end{aligned} \quad (22)$$

\mathbf{W}_{ij} is the auxiliary variable in this case. The first two constraints ensure \mathbf{I} is a permutation matrix, the third constraint ensures \mathbf{I} to be binary. The last two constraints come from $\mathbf{W}_{ij} = \min(\mathbf{D}_{ij}, \mathbf{I}_{ij})$. In such way we turn such "min" into two conditions in the optimization. Such optimization can be efficiently solved by MILP algorithms. The algorithm returns \mathbf{I} and \mathbf{W} simultaneously and we only use \mathbf{I} in the following steps.

With the most similar permutation matrix, the next step is to generate a tree from such matrix by a sequence of dilation. From Property 5, we know there are $(N+1)^{N-1}$ trees can be generated, which is still a large number. We leverage the Trellis algorithm that only performs one-step dilation and retain the matrices with the smallest Hamming distance. We cut the branches with high Hamming distances that they are unlikely to generate the tree we need. The algorithm is summarized in algorithm 3. We show an example running such algorithm in Appendix Q.

I. Application in Robotics

Here we briefly explain how such theory can be used in real robot applications. In section III-B and III-D, we have shown how an open-chain robot can be reduced to a heterogeneous out-tree, and such out-tree is a valid representation of robot topology. However, if we cannot directly observe such topology, we have to infer such topology by some observations from other sources. In this paper, we assume the "other sources" are exteroception and proprioception data, which are measured by full-body IMUs and joint encoders. From such measurements, we can extract a binary heterogeneous dependency matrix. Theorem 1 and 2 tells us such matrix is a complete representation of heterogeneous out-tree we want to know, which represents the robot topology. Then we discussed the partially observable case, which is that for some links, there is no sensor mounted on. Theorem 3 tells us when such partial observed data can be reconstructed to a heterogeneous out-tree and when such reconstruction is unique. The matrix correction algorithm ensures when the heterogeneous dependency matrix is erroneous, how we can still correct it and extract the tree structure.

Such mechanism could have significant potential in robotics. First, the mechanism can monitor the body structure of the robot, when the robot body is damaged, our algorithm will identify that the body topology has changed and give a damage warning. Also, for some robots with unknown body structures or some robots whose FKs are hard to model (like soft robots), our work can find the most similar rigid body topology that describes the unknown body structure.

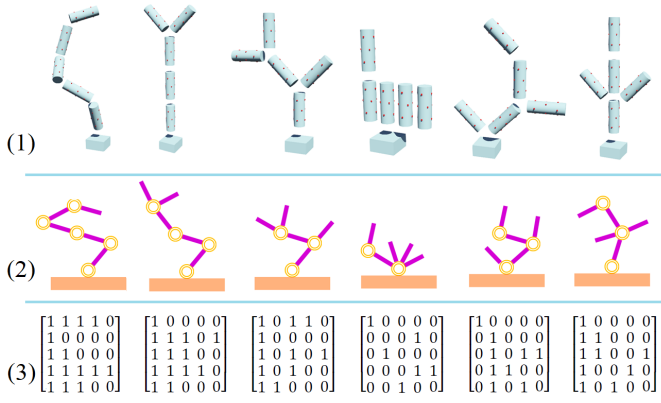


Fig. 10: (1) Different robot topology in experiment. Red dots on robot body are IMUs. (2) the recognized robot body structures; (3) the extracted heterogeneous dependency matrices.

IV. EXPERIMENTS

A. Simulation

For the experiments, we designed 6 open-chain robots in Webots simulator with different body structures (Figure 10 (1)). Each robot has 5 links except the base link and with 5 joints. 12 IMUs are evenly distributed on the surface of each link. The z-axis of IMU is pointing outwards the link along the surface normal while x and y axes are chosen arbitrarily. To record data, we perform random motion on each joint, which means every 0.2 seconds, we cast a uniformly distributed torque on each joint and keep the torque constant in such period. The sampling frequency is 100 Hz. The result of running our algorithm is shown in Figure 10 (2-3). Our algorithm correctly identify the ground-truth robot body structures as (1) by extracting heterogeneous dependency matrices as shown in (3).

B. Baselines Comparison

We compared work from [21] with the six robots in the last sub-section, the result is shown in Figure 11. Results of their method using their original tactile data is marked as BS-Tac and using our IMU data is marked as BS-IMU. The dimension of Multidimensional scaling (MDS) in their method is set as $d = 10$, which means the original signal is mapped to 10 dimension space. We use mutual information to estimate the information metric D in their work.

The sensor clustering and topology recognition are shown in Figure 11 (a, b). The yellow nodes represent recognized links and yellow edges are recognized joints. Due to the original 10-D mapping is then reduced to 2-D for plotting, each cluster may not connect to its nearest cluster in 2D space. Comparing BS-Tac and BS-IMU, we can find that their algorithm clustering in BS-Tac but the clustering is not clear in BS-IMU, which means their work has weaker distinguishing ability with local information such as IMU signal.

The right side of Figure 11 shows the recognized topology of our solution and theirs. Different from our solution, their work finds the undirected graphs as Figure 11 (e,f) while ours finds the out-tree structure Figure 11 (d). The color of links

joint name	A_i	k_i	y_i
shoulder_pan_joint	0.2	0.1	0.1
shoulder_lift_joint	0.2	0.13	0.2
elbow_joint	0.2	0.15	0.3
wrist_1_joint	0.2	0.17	0.4
wrist_2_joint	0.2	0.19	0.5
wrist_3_joint	0.2	0.21	0.6

TABLE I: Real robot joint velocity trajectory parameters.

are used to mark different labels, and they are consistent in all figures. In the last column, all links are marked grey, because the algorithm cannot cluster the sensors and find their correspondence correctly. Clearly, our work reconstructs the topology precisely, but the baselines only captures the topology correctly with only a small fraction of body parts. Also, some links are wrongly connected, as robot 2 red and purple link. As IMU data is a highly non-linear mapping from joint values, it is arguable to use a information metric extracted from data to directly represent the interconnection between clustering, as their work uses to find the latent joints. This might be the reason that their work shows clustering performance with tactile data extracted from global information (see more details in [21]), but in BS-IMU, clustering is less recognizable Figure 11 (b).

The clustering result is more clear in Figure 12. Both our solution and [21] employed DPGMM, so we can compare the clustering results with the ground-truth clustering, as the correspondence between sensors and links is known (which sensor is connected to which link). From Figure 12, we see our solution preserves the ground-truth clustering well. However the clustering in BS-IMU is almost random. It means that their method can hardly find the correspondence between sensors and links with only IMU data. It is the reason that in Figure 11, the links are marked with grey.

C. Real Robot Test

We tested our algorithm on a UR5e robot arm. We mount two MPU6050 sensors on each link (Figure 13a-13b). The robot is programmed to track sinusoidal joint velocities as Equation 23.

$$\dot{q}(t) = A_i \cdot \sin(2\pi k_i \cdot t + y_i) \quad (23)$$

The parameters A_i , k_i and y_i chosen are shown in Table I, i is the index for the joints in Table I. As the real robot is affected by gravity that introduces additional acceleration term, Equation 11 shall be modified to cancel out the gravity effect, which becomes Equation 24.

$$\phi^* = \underset{\phi}{\operatorname{argmin}} \left[\left| \alpha_B - \mathbf{R}^T \mathbf{g} - \mathbf{R}^T \ddot{\mathbf{b}} \right| - \operatorname{tr}(\mathbf{R}_1^T \mathbf{R}_2) \right] \quad (24)$$

\mathbf{g} is the gravity vector that is usually set as $\mathbf{g} = [0, 0, -9.8]^T$. The recognized body structure is shown in Figure 13c. From that we see our algorithm successfully recognized the UR5e robot body topology but baseline [21] failed to.

D. Neural Network Structure Comparison

To show the advantage of our neural network structure proposed in Figure 2, we compared with a multi-layer perceptrons (MLP) regressor. For each sensor on the robot, there

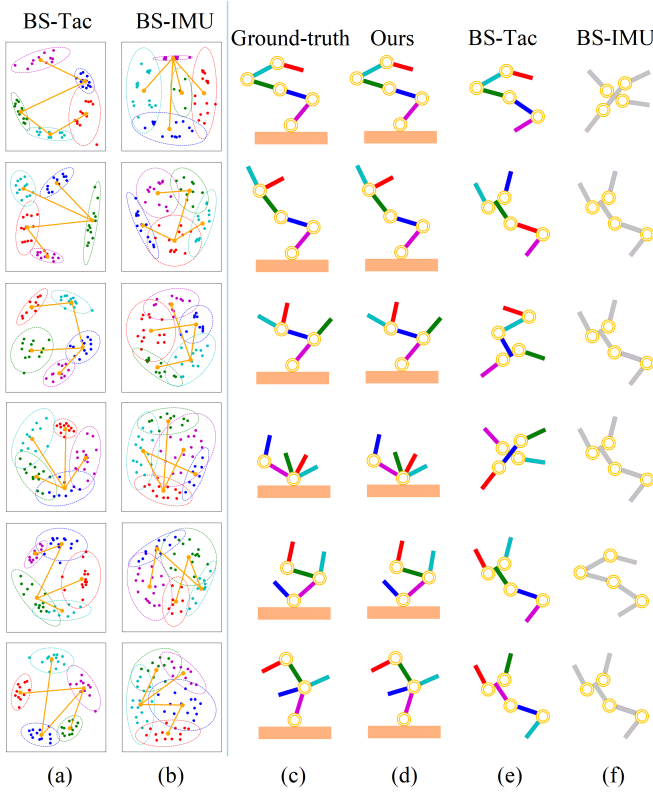


Fig. 11: Body schema recognition: (a) clustering and body schema recognition results of [21] using tactile signal; (b) results of [21] using IMU signal. Yellow nodes represent recognized links and yellow edges are recognized joints; (c) ground-truth topology; (d) results of our solution; (e) results of [21] using tactile signal; (f) results of [21] using IMU signal. Colors show the link correspondence.

is an independent MLP regressor attached to it. The network structure is shown in Figure 14a. The input of neural network is joint angles θ , velocities $\dot{\theta}$ and accelerations $\ddot{\theta}$, the outputs are predicted body linear accelerations $\overline{\alpha_B} \in \mathbb{R}^3$ and body angular velocities $\overline{\beta_B} \in \mathbb{R}^3$. The neural network weights are trained by minimizing the following loss function

$$\phi^* = \underset{\phi}{\operatorname{argmin}} (\|\alpha_B - \overline{\alpha_B}\| + \|\beta_B - \overline{\beta_B}\|) \quad (25)$$

where α_B , β_B are measured body linear accelerations and body angular velocities from IMUs. The Jacobian of such network is $\frac{\partial(\overline{\alpha_B}, \overline{\beta_B})}{\partial(\theta, \dot{\theta}, \ddot{\theta})} \in \mathbb{R}^{6 \times 3n}$. We only use the joint angles part $\frac{\partial(\overline{\alpha_B}, \overline{\beta_B})}{\partial\theta} \in \mathbb{R}^{6 \times n}$. The sliced Jacobians are then processed by Equation 16-19 to extract the corresponding Heterogeneous Dependency Matrix of the robot. The results are shown in Figure 14b. From the result, we see MLP is not capable of learning the correct tree structures.

V. CONCLUSION

In this work, we proposed an algorithm for an open-chain robot with full-body exteroception and proprioception sensors to recognize its body structure. The exteroception signal is

measured by IMUs and the proprioception signal is measured by joint encoders. We assigned each on-body sensor a neural network and proposed a training method to learn the global poses of the sensors. The Jacobian of such neural networks encodes dependency information which can be formed as a heterogeneous dependency matrix. We can also extract a heterogeneous out-tree structure from each robot that represents its body structure. We showed such matrix and out-tree are equivalent representations of the robot body topology. As such matrix comprises a subset of all binary square matrices, we proved two theorems that give the condition when a binary square matrix is a heterogeneous dependency matrix and discussed the remedy to fix such matrix when it is contaminated by partial observability and data noise. The simulation result showed that our algorithm successfully identified the body structures of 6 different robots with different skeletons and was validated on an UR5e real platform. The potential application of our algorithm is to identify the forward kinematics of robots whose forward kinematics is not accessible or hard to model. It is a big step for a robot to recognize itself instead of only interacting with the environment. The future work includes extending such algorithm to locomotion robot scenarios, shortening the time of training to make it more fast-adaptive.

APPENDIX

APPENDIX A

DETAILED DERIVATION OF EXTEROCEPTION ESTIMATION

Assuming we have a second-order differentiable function approximator $f_\phi(\theta)$

$$f_\phi(\theta) = \mathbf{T}_\phi(\theta) = \begin{bmatrix} \mathbf{R}(\theta) & \mathbf{b}(\theta) \\ \mathbf{0} & 1 \end{bmatrix} \quad (26)$$

which is parameterized by ϕ . The function approximator is used to map the input joint angle vector θ to a homogeneous transformation $\mathbf{T}_\phi(\theta)$ in SE(3) that characterizes the transformation that sensor frame B described in global frame G . Reader should keep in mind that for each sensor on the robot body, there will be a unique $f_\phi(\theta)$ to represent the sensor, we only discuss one of them, and the rest are used as the same way. Due to lacking of the knowledge of the robot body structure, the ground-truth homogeneous transformation is unknown, that is why we use such an approximator. We denote the first and second-order derivative of $f_\phi(\theta)$ as $\frac{\partial f_\phi(\theta)}{\partial\theta} = \mathbf{J}_\phi(\theta) \in \mathbb{R}^{4 \times 4 \times N}$ and $\frac{\partial^2 f_\phi(\theta)}{\partial\theta^2} = \mathbf{H}_\phi(\theta) \in \mathbb{R}^{4 \times 4 \times N \times N}$, where N is the number of joints. We can also measure the proprioception as the angles, angular velocities and angular accelerations for all the joint angles (though we do not know their hierarchy) as θ , $\dot{\theta}$, $\ddot{\theta}$. The exteroception data are the vectors $[\alpha_B, \beta_B]^T$ of linear acceleration and angular velocity (by roll-pitch-yaw) described in body frame, where $\alpha_B \in \mathbb{R}^3$, $\beta_B \in \mathbb{R}^3$. We will ignore the symbol of dependency of θ for all variables to make the result neat. The first and second-order time derivative of $f_\phi(\theta)$ are shown in Equations 27 and 29.

$$\frac{\partial f_\phi}{\partial t} = \frac{\partial f_\phi}{\partial \theta} \frac{\partial \theta}{\partial t} = \mathbf{J}_\phi \dot{\theta} = \begin{bmatrix} \dot{\mathbf{R}} & \dot{\mathbf{b}} \\ \mathbf{0} & 1 \end{bmatrix} \quad (27)$$

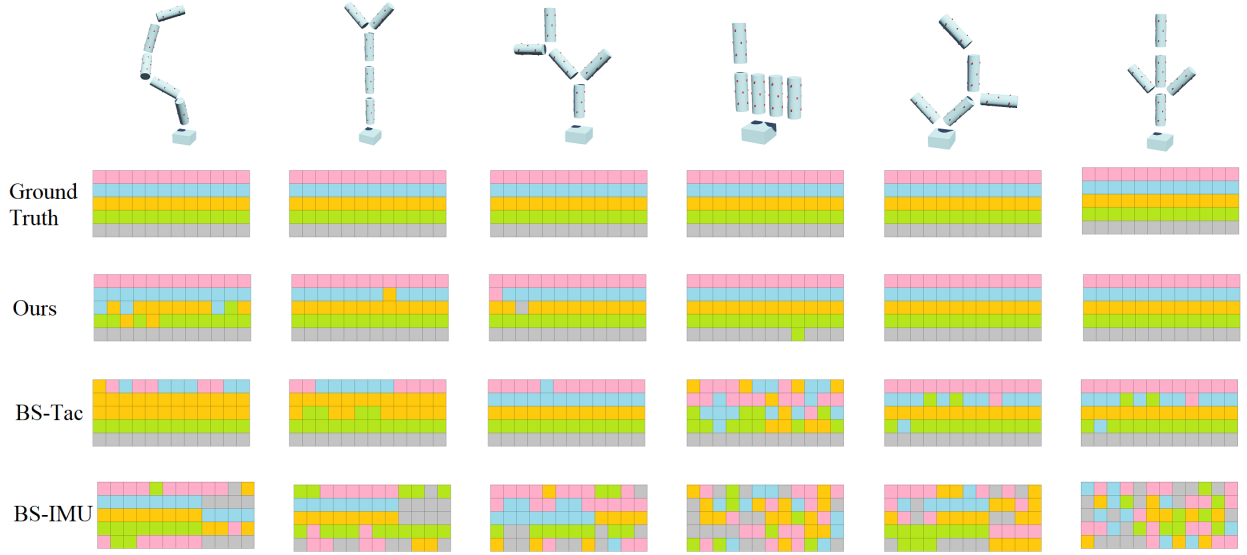


Fig. 12: Clustering results of DPGMM components.

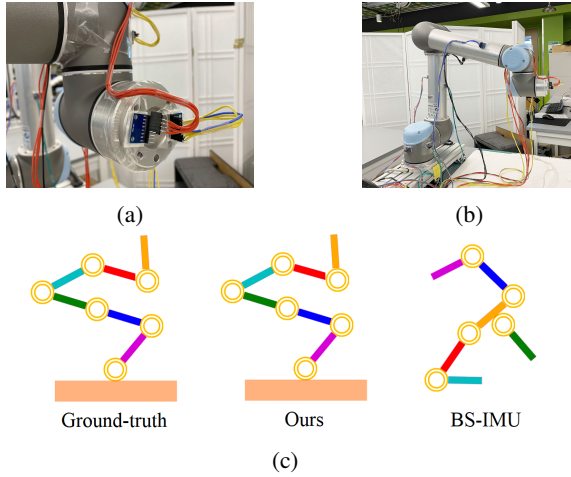


Fig. 13: (a) MPU6050 mounting. (b) Robot with full-body IMUs. (c) Ground-truth and recognized robot body structure by our algorithm and baseline [21].

$$\begin{aligned}
 \frac{\partial^2 f_\phi}{\partial t^2} &= \frac{\partial}{\partial t} \left(\frac{\partial f_\phi}{\partial t} \right) \\
 &= \frac{\partial}{\partial t} \left(\frac{\partial f_\phi}{\partial \theta} \frac{\partial \theta}{\partial t} \right) \\
 &= \frac{\partial}{\partial t} (\mathbf{J}_\phi \dot{\theta}) \\
 &= \left(\frac{\partial \mathbf{J}_\phi}{\partial t} \right) \dot{\theta} + \mathbf{J}_\phi \ddot{\theta} \\
 &= \left(\frac{\partial \mathbf{J}_\phi}{\partial \theta} \frac{\partial \theta}{\partial t} \right) \dot{\theta} + \mathbf{J}_\phi \ddot{\theta} \\
 &= \begin{bmatrix} \ddot{\mathbf{R}} & \ddot{\mathbf{b}} \\ \mathbf{0} & 1 \end{bmatrix} = \mathbf{H}_\phi \dot{\theta} \dot{\theta} + \mathbf{J}_\phi \ddot{\theta}
 \end{aligned} \tag{28}$$

and

Define operation

$$\begin{bmatrix} w_1 \\ w_2 \\ w_3 \end{bmatrix}^\wedge = \begin{bmatrix} 0 & -w_3 & w_2 \\ w_3 & 0 & -w_1 \\ -w_2 & w_1 & 0 \end{bmatrix} \tag{33}$$

$$\begin{bmatrix} 0 & -w_3 & w_2 \\ w_3 & 0 & -w_1 \\ -w_2 & w_1 & 0 \end{bmatrix}^\vee = \begin{bmatrix} w_1 \\ w_2 \\ w_3 \end{bmatrix} \tag{34}$$

We conclude that the linear part α_B equals $\mathbf{R}^T \ddot{\mathbf{b}}$ because they are both in \mathbb{R}^3 . To find the expression of β_B , from $r_G = \mathbf{T}_\phi \cdot r_B$, we have

$$\dot{r}_G = \dot{\mathbf{T}}_\phi \cdot r_B = \dot{\mathbf{T}}_\phi \cdot \mathbf{T}_\phi^{-1} \cdot r_G = \begin{bmatrix} \dot{\mathbf{R}} \mathbf{R}^T & \dot{\mathbf{b}} - \dot{\mathbf{R}} \mathbf{R}^T \mathbf{b} \\ \mathbf{0} & 0 \end{bmatrix} \cdot r_G \tag{35}$$

find the relation between \mathbf{R} , \mathbf{b} , $\dot{\mathbf{R}}$, $\dot{\mathbf{b}}$, $\ddot{\mathbf{R}}$, $\ddot{\mathbf{b}}$ and $[\alpha_B, \beta_B]^T$.

For any point r in space, we have

$$r_G = \mathbf{T}_\phi \cdot r_B \tag{30}$$

r_G and r_B are coordinates of r in global and sensor frame respectively. Take the second-order time derivative of such relation, we have

$$a_G = \ddot{r}_G = \ddot{\mathbf{T}}_\phi \cdot r_B = \begin{bmatrix} \ddot{\mathbf{R}} & \ddot{\mathbf{b}} \\ \mathbf{0} & 0 \end{bmatrix} \cdot r_B \tag{31}$$

so the acceleration of point r in body frame is

$$\begin{aligned}
 a_B &= \mathbf{T}_\phi^{-1} a_G = \mathbf{T}_\phi^{-1} \cdot \ddot{\mathbf{T}}_\phi \cdot r_B \\
 &= \begin{bmatrix} \mathbf{R}^T & -\mathbf{R}^T \mathbf{b} \\ \mathbf{0} & 1 \end{bmatrix} \cdot \begin{bmatrix} \ddot{\mathbf{R}} & \ddot{\mathbf{b}} \\ \mathbf{0} & 0 \end{bmatrix} \cdot r_B \\
 &= \begin{bmatrix} \mathbf{R}^T \ddot{\mathbf{R}} & \mathbf{R}^T \ddot{\mathbf{b}} \\ \mathbf{0} & 0 \end{bmatrix} \cdot r_B
 \end{aligned} \tag{32}$$

The two equations show we can find $\dot{\mathbf{R}}$, $\dot{\mathbf{b}}$, $\ddot{\mathbf{R}}$ and $\ddot{\mathbf{b}}$ from exteroception and proprioception data. The next step is to

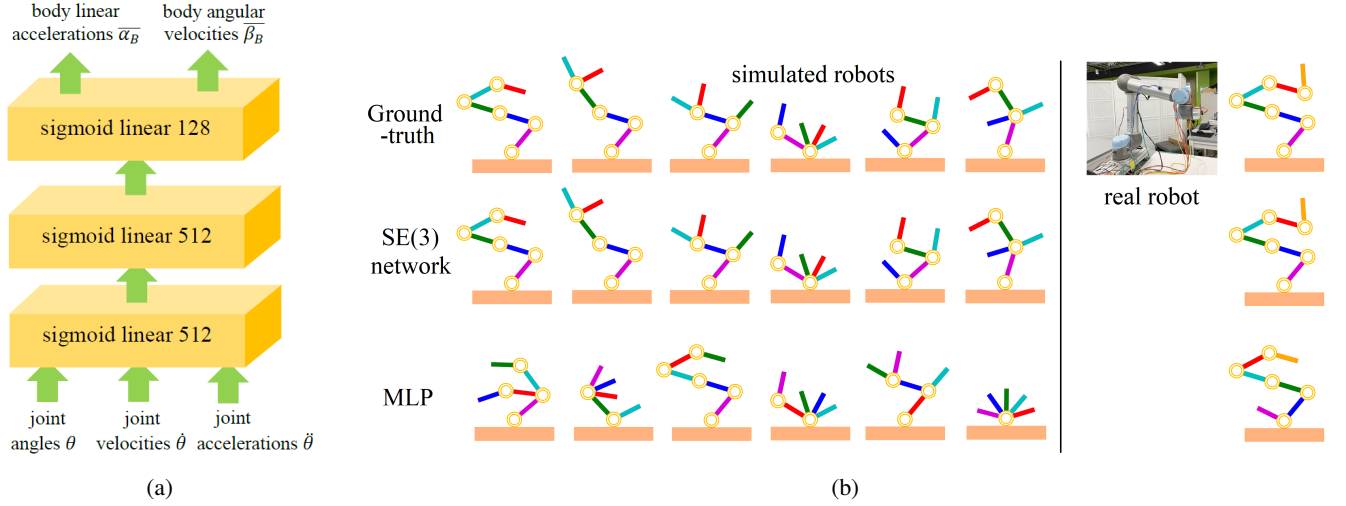


Fig. 14: (a) Neural network structure of multi-layer perceptrons (MLP) regressor. (b) Heterogeneous Out-tree extraction results of simulated robots and real robot. (top row) ground-truth tree structure; (middle row) tree structure extracted using the proposed SE(3) network; (bottom row) tree structure extracted using MLP network.

Define global angular velocity matrix as $\omega_G^\wedge = \dot{\mathbf{R}}\mathbf{R}^T$. Apparently $\omega_G^\wedge \in \mathfrak{so}(3)$ and the corresponding global angular velocity is $\omega_G \in \mathbb{R}^3$. We know for any vector v ,

$$(\mathbf{R} \cdot v)^\wedge = \mathbf{R} \cdot v^\wedge \cdot \mathbf{R}^T \quad (36)$$

We know the relation $\omega_G = \mathbf{R}\omega_B$ as ω_G and ω_B are the same vector expressed in different frames. By Equation 36, we have

$$\omega_B^\wedge = \mathbf{R}^{-1}\omega_G^\wedge\mathbf{R} = \mathbf{R}^{-1}\dot{\mathbf{R}}\mathbf{R}^T\mathbf{R} = \mathbf{R}^T\dot{\mathbf{R}} \quad (37)$$

However, the corresponding vector ω_B is not β_B because ω_B is the rotation velocity vector described by axis-angle system and β_B is the rotation velocity vector described by roll-pitch-yaw system. To align the two representations, we know the two velocity vectors should cause the same rotation effect in a short period of time T_s . For ω_B , it can be decomposed to a time derivative of angle $\dot{\vartheta} \in \mathbb{R}$ and a rotation axis vector $\vec{u} \in \mathbb{R}^3$, with $\omega_B = \dot{\vartheta}\vec{u}$ and $|\vec{u}| = 1$. The rotated angle in T_s can be approximated as $\dot{\vartheta}T_s$. By Rodrigues' rotation formula, the corresponding rotation matrix in T_s is

$$\mathbf{R}_1 = \mathbf{I} + \sin(\dot{\vartheta}T_s)\omega_B^\wedge + [1 - \cos(\dot{\vartheta}T_s)]\omega_B^\wedge \cdot \omega_B^\wedge \quad (38)$$

For β_B , it represents the roll, pitch, yaw velocities as $\beta_B = [\beta_{B1}, \beta_{B2}, \beta_{B3}]^T$. The rotation angle in T_s can be approximated by $[\beta_{B1}T_s, \beta_{B2}T_s, \beta_{B3}T_s]^T$, so the rotation matrix is calculated from standard roll-pitch-yaw matrices as

$$\begin{aligned} \mathbf{R}_2 &= \mathbf{R}_z(\beta_{B3}T_s)\mathbf{R}_y(\beta_{B2}T_s)\mathbf{R}_x(\beta_{B1}T_s) \\ &= \begin{bmatrix} a_{00} & a_{01} & a_{02} \\ a_{10} & a_{11} & a_{12} \\ a_{20} & a_{21} & a_{22} \end{bmatrix} \end{aligned} \quad (39)$$

with

$$\begin{aligned} a_{00} &= \cos(\beta_{B3}T_s)\cos(\beta_{B2}T_s) \\ a_{01} &= \cos(\beta_{B3}T_s)\sin(\beta_{B2}T_s)\sin(\beta_{B1}T_s) - \sin(\beta_{B3}T_s)\cos(\beta_{B1}T_s) \\ a_{02} &= \cos(\beta_{B3}T_s)\sin(\beta_{B2}T_s)\cos(\beta_{B1}T_s) + \sin(\beta_{B3}T_s)\sin(\beta_{B1}T_s) \\ a_{10} &= \sin(\beta_{B3}T_s)\cos(\beta_{B2}T_s) \\ a_{11} &= \sin(\beta_{B3}T_s)\sin(\beta_{B2}T_s)\sin(\beta_{B1}T_s) + \cos(\beta_{B3}T_s)\cos(\beta_{B1}T_s) \\ a_{12} &= \sin(\beta_{B3}T_s)\sin(\beta_{B2}T_s)\cos(\beta_{B1}T_s) - \cos(\beta_{B3}T_s)\sin(\beta_{B1}T_s) \\ a_{20} &= -\sin(\beta_{B2}T_s) \\ a_{21} &= \cos(\beta_{B2}T_s)\sin(\beta_{B1}T_s) \\ a_{22} &= \cos(\beta_{B2}T_s)\cos(\beta_{B1}T_s) \end{aligned} \quad (40)$$

APPENDIX B PROOF OF PROPOSITION 1

Proposition 1 Transform Invariant Jacobian is invariant to any transformation \mathbf{Y} .

Proof: Similarly, we represent sensor frame \mathbf{T} as

$$\mathbf{T} = \begin{bmatrix} \mathbf{n}_x & \mathbf{n}_y & \mathbf{n}_z & \mathbf{b} \\ 0 & 0 & 0 & 1 \end{bmatrix} \quad (41)$$

$\mathbf{n}_x, \mathbf{n}_y, \mathbf{n}_z$ are unit vectors of each axis, and \mathbf{b} is the global position. We have an arbitrary transformation \mathbf{Y} as

$$\mathbf{Y} = \begin{bmatrix} \mathbf{R}' & \mathbf{b}' \\ \mathbf{0} & 1 \end{bmatrix} \quad (42)$$

The transformed new frame is

$$\mathbf{T}' = \mathbf{Y} \cdot \mathbf{T} = \begin{bmatrix} \mathbf{n}'_x(\theta) & \mathbf{n}'_y(\theta) & \mathbf{n}'_z(\theta) & \mathbf{b}''(\theta) \\ 0 & 0 & 0 & 1 \end{bmatrix} \quad (43)$$

with $\mathbf{n}'_x(\theta) = \mathbf{R}' \cdot \mathbf{n}_x(\theta)$,
 $\mathbf{n}'_y(\theta) = \mathbf{R}' \cdot \mathbf{n}_y(\theta)$,
 $\mathbf{n}'_z(\theta) = \mathbf{R}' \cdot \mathbf{n}_z(\theta)$,
 $\mathbf{b}''(\theta) = \mathbf{R}' \cdot \mathbf{b}(\theta) + \mathbf{b}'$

The new Jacobians are:

$$\begin{aligned}\frac{\partial \mathbf{n}'_x(\theta)}{\partial \theta} &= \mathbf{R}' \frac{\partial \mathbf{n}_x(\theta)}{\partial \theta} \\ \frac{\partial \mathbf{n}'_y(\theta)}{\partial \theta} &= \mathbf{R}' \frac{\partial \mathbf{n}_y(\theta)}{\partial \theta} \\ \frac{\partial \mathbf{n}'_z(\theta)}{\partial \theta} &= \mathbf{R}' \frac{\partial \mathbf{n}_z(\theta)}{\partial \theta} \\ \frac{\partial \mathbf{r}'(\theta)}{\partial \theta} &= \mathbf{R}' \frac{\partial \mathbf{r}(\theta)}{\partial \theta}\end{aligned}$$

Because \mathbf{R}' is unitary matrix, we have $\left| \frac{\partial \mathbf{n}'_x(\theta)}{\partial \theta} \right| = \left| \frac{\partial \mathbf{n}_x(\theta)}{\partial \theta} \right|$,

$$\begin{aligned}\left| \frac{\partial \mathbf{n}'_y(\theta)}{\partial \theta} \right| &= \left| \frac{\partial \mathbf{n}_y(\theta)}{\partial \theta} \right|, \\ \left| \frac{\partial \mathbf{n}'_z(\theta)}{\partial \theta} \right| &= \left| \frac{\partial \mathbf{n}_z(\theta)}{\partial \theta} \right|, \\ \left| \frac{\partial \mathbf{b}'(\theta)}{\partial \theta} \right| &= \left| \frac{\partial \mathbf{b}(\theta)}{\partial \theta} \right|\end{aligned}$$

end of proof.

APPENDIX C

PROOF OF PROPERTY 2

Property 2 Rows and columns of \mathbf{D} are non-duplicate.

Proof: When we construct matrix \mathbf{D} , we eliminate all duplicate rows, so there are no duplicate rows. Because each element \mathbf{D}_{ij} records if the path from node i to root passes edge j or not, any column j of \mathbf{D} represents the collection of indices of all descendants of edge j . Because one edge is only connecting to one child node directly, such child node must be the root node of the sub-tree constructed by this collection (though we don't exactly know which node it is connecting, it should be one in the collection). If another edge k has the same column, similarly, the child node connects to edge k must be the root node of the sub-tree constructed by that collection. We know two edges j and k cannot connect to the same child node, which means duplicate column introduces two root nodes to the same sub-tree, which is not possible.

end of proof.

APPENDIX D

PROOF OF PROPERTY 5

Property 5 There are $(N+1)^{N-1} \cdot N!$ different tree structures with N nodes.

Proof: From Cayley's Formula, the number of trees without edge labels is $(N+1)^{N-1}$. Then we take node-edge pairing, there are $N!$ different ways of pairing N nodes and N edges.

end of proof.

APPENDIX E

PROOF OF LEMMA 1

Lemma 1 From each heterogeneous out-tree, one can extract a determined heterogeneous dependency matrix.

Proof: Because it is an out-tree, for each node i in the tree, one can find a unique route from i to the root. As all rows of the matrix are labelled, each node i corresponds to a particular row in the matrix. All edges j that the route passes will set the j -th element in row i to one while keeping the unvisited edges zero. In such way, one can construct a determined heterogeneous dependency matrix.

end of proof.

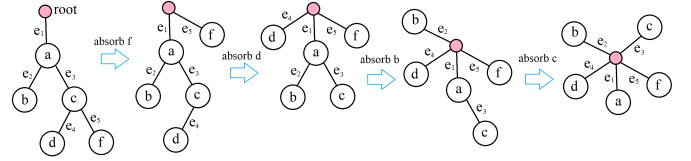


Fig. 15: Demonstration of using absorption operation to transform a tree to a depth-1 tree

APPENDIX F

PROOF OF LEMMA 2

Lemma 2 $ab^{j \rightarrow i}(t)$ and $di^{i \rightarrow j}(t)$ on heterogeneous out-tree set are a pair of inverse operation.

Proof: Absorption moves a leaf node and its direct parent edge to the root while dilation moves a leaf node and its direct parent edge back to the original position without changing the topology of other parts of the tree.

end of proof.

APPENDIX G

PROOF OF PROPOSITION 2

Proposition 2 Any tree t can be transformed to a depth-1 tree by a series of absorption and from the depth-1 tree, reconstruct the original tree t .

Proof: A depth-1 tree is a star shape graph that each node is directly connecting to the root. We know that for any heterogeneous out-tree, the absorption operation is to move a node with its parent edge to the root. We can design an algorithm that first moves all leaf nodes to the root. Then the old leaf nodes are all depth-1, and some new nodes become leaf nodes. We repeat such operation of absorbing leaf nodes until all nodes are depth-1 (Figure 15). Due to Lemma 2,

Lemma 2: $ab^{j \rightarrow i}(t)$ and $di^{i \rightarrow j}(t)$ on heterogeneous out-tree set are a pair of inverse operation.

we can find the reversed sequence of dilation operation to reconstruct such tree.

end of proof.

APPENDIX H

PROOF OF COROLLARY 1

Corollary 1 Tree set \mathbb{T}_N is closed under dilation and absorption.

Proof: From the definition of dilation and absorption, moving a deeper leaf node to the root or moving a root-connected leaf to a deeper position will still result in a tree.

end of proof.

APPENDIX I

PROOF OF PROPOSITION 3

Proposition 3 For any heterogeneous out-tree $t \in \mathbb{T}_N$ and its generated heterogeneous dependency matrix $\mathbf{D} \in \mathbb{D}_N$,

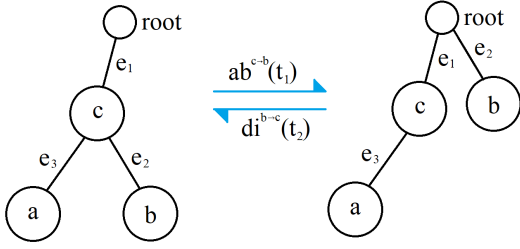


Fig. 16: Demonstration of dilation $di^{i \rightarrow j}(t)$ and absorption $ab^{j \rightarrow i}(t)$.

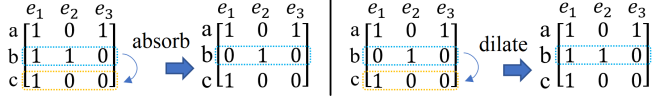


Fig. 17: Absorption and dilation on matrix set. Matrices correspond to trees in Figure 6a.

absorption operation on t is equivalent to absorption operation on \mathbf{D} . So as for dilation.

Proof: Because $\mathbf{D} \in \mathbb{D}_N \subseteq \mathbb{S}_N$, operations defined on \mathbb{S}_N also apply to \mathbf{D} . We are aware of a fact that if node i is a child of node j , row \mathbf{D}_i will have one more "1" than row \mathbf{D}_j and all other entries the same. $\mathbf{S}_i - \mathbf{S}_j$ in absorption operation makes \mathbf{D}_j get rid of all the dependencies introduced by \mathbf{D}_j , and only leave the dependency of \mathbf{D}_i 's parent edge. This operation makes the new \mathbf{D}_i has only one "1", which indicates it directly connects to the root. The operation is equivalent to move node i from child of j to the root along with its edge.

For dilation operation, we ensure there is only one "1" in \mathbf{D}_i so that \mathbf{D}_i is originally connected to the root. $\mathbf{S}_i + \mathbf{S}_j$ in dilation operation makes \mathbf{D}_i inherits all dependencies of \mathbf{D}_j . Because we originally ensure $\mathbf{S}_i \cap \mathbf{S}_j = 0$, the new \mathbf{D}_i will have one more "1" than \mathbf{D}_j , which means $\text{depth}(\mathbf{D}_i) = \text{depth}(\mathbf{D}_j) + 1$, \mathbf{D}_i becomes the direct child of \mathbf{D}_j . The operation is equivalent to move node i from the root to the child of j along with its edge. The equivalence of absorption and dilation on tree set and matrix set are shown in Figure 6a and 17.

Thus, we can see absorption and dilation defined in \mathbb{D}_N and \mathbb{S}_N are equivalent.

end of proof.

APPENDIX J PROOF OF PROPOSITION 4

Proposition 4 *The tree to matrix translation in Lemma 1 is bijective.*

Proof: Injective:
From Lemma 1,

Lemma 1: *From each heterogeneous out-tree, one can extract a determined heterogeneous dependency matrix.*

we know for each $t \in \mathbb{T}_N$, there is $\mathbf{D} \in \mathbb{D}_N$. What we need to show is for $t_1, t_2 \in \mathbb{T}_N$ and $t_1 \neq t_2$, their

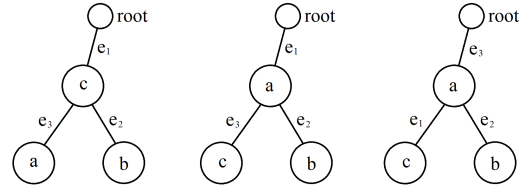


Fig. 18: Examples of heterogeneous out-tree.

counterparts $\mathbf{D}_1, \mathbf{D}_2 \in \mathbb{D}_N$ are different, which is $\mathbf{D}_1 \neq \mathbf{D}_2$. To show such distinction, we first segment \mathbb{D}_N by semi-equivalent defined in Definition 5.

Definition 5: *Two heterogeneous out-trees are semi-equivalent if any node with the same label in both trees has the same parent node.*

For example, tree 1 in Figure 5c is in one subset and tree 2, 3 in are in another subset. In each subset, there is a set of trees share the same node-only topology as traditional out-tree. If the two trees t_1 and t_2 are different out-tree, at some where in the tree should we find the first pair of parent a and its child b (by search algorithm as BFS) that only found in t_1 but in t_2 .

- in t_1 : $a \rightarrow b$
- in t_2 : $a \not\rightarrow b$

We can separate this into two conditions:

1) b is a descendant of a (not child) in t_2 but b is a child of a in t_1 : in t_1 case, $\text{depth}(b) = \text{depth}(a) + 1$. In t_2 case, b is attached to the sub-tree rooted on a , $\text{depth}(b) > \text{depth}(a) + 1$. By property 4,

Property 4: $\sum_j \mathbf{D}_{ij}$ is the depth of node i in the tree.

there must be $\sum_j \mathbf{D}_{2b,j} > \sum_j \mathbf{D}_{1b,j}$. Thus $\mathbf{D}_1 \neq \mathbf{D}_2$.

2) b is not a descendant of a in t_2 but b is a child of a in t_1 . in t_1 case, b inherits dependency of a , so $\mathbf{D}_{1b,a} = 1$. In t_2 case, because a, b is the first error pair found, b cannot be an ascendant of a . So, b must be on a other sub-tree which does not include a , which means b has no dependency on a , $\mathbf{D}_{2b,a} = 0$. $\mathbf{D}_1 \neq \mathbf{D}_2$

Next, we discuss trees in each subset considering its dependency on edges. This problem is that given an out-tree without edge labels, how to fit different edge label to each edge. Apparently there are $N!$ possible assignments considering all permutations of edge labels as shown in Figure 8. From property 2,

Property 2: *Rows and columns of \mathbf{D} are non-duplicate.*

we know that no columns are duplicate, so each of the assignment will result in a unique matrix \mathbf{D} .

To summarize, subset in \mathbb{T}_N separated by semi-equivalence will result in non-duplicate \mathbf{D} while in each subset, all the elements have non-duplicate \mathbf{D} . This implies for each tree,

$$\begin{array}{c} \begin{array}{ccc} & d & e & f \\ \begin{array}{c} a \\ b \\ c \end{array} & \begin{bmatrix} 1 & 0 & 0 \\ 0 & 1 & 0 \\ 0 & 0 & 1 \end{bmatrix} \end{array} & \neq & \begin{array}{ccc} & d & f & e \\ \begin{array}{c} a \\ b \\ c \end{array} & \begin{bmatrix} 1 & 0 & 0 \\ 0 & 1 & 0 \\ 0 & 0 & 1 \end{bmatrix} \end{array} \end{array}$$

Fig. 19: Different permutation matrices

the extraction will map it to a unique matrix $\mathbf{D} \in \mathbb{D}_N$.

Surjective:

From the definition of \mathbf{D} , we know there is must be a tree that generate such matrix, so each matrix must have a preimage in \mathbb{T}_N .

end of proof.

APPENDIX K PROOF OF THEOREM 1

We first prove a lemma.

Lemma 3. *A heterogeneous dependency matrix as a permutation matrix can be extracted from a depth-1 tree.*

Proof: From Lemma 1,

Lemma 1: *From each heterogeneous out-tree, one can extract a determined heterogeneous dependency matrix.*

we can extract a determined heterogeneous dependency matrix from depth-1 tree. From property 4,

Property 4: $\sum_j \mathbf{D}_{ij}$ is the depth of node i in the tree.

we know each row has only one element as 1 and others are all zero. From property 2,

Property 2: *Rows and columns of \mathbf{D} are non-duplicate.*

we know the element "1"s in different rows are separated into different columns. Thus, by property 1,

Property 1: *Rows and columns of \mathbf{D} are interchangeable.*

we can rearrange the matrix to a permutation matrix.
end of proof.

Theorem 1 *For any binary matrix $\mathbf{D} \in \{0,1\}^{N \times N}$, it has unique corresponding heterogeneous out-tree iff it can be transformed to an permutation matrix \mathbf{I} by a sequence of adsorption and dilation.*

Proof: $t \Rightarrow \mathbf{I}$:

Combining proposition 2, lemma 3 and proposition 3,

Proposition 2: *Any tree t can be transformed to a depth-1 tree by a series of absorption and from the depth-1 tree, reconstruct the original tree t .*

Lemma 3: *A heterogeneous dependency matrix as a permutation matrix can be extracted from a depth-1 tree.*

Proposition 3: *For any heterogeneous out-tree $t \in \mathbb{T}_N$ and its generated heterogeneous dependency matrix $\mathbf{D} \in \mathbb{D}_N$, absorption operation on t is equivalent to absorption operation on \mathbf{D} . So as for dilation.*

we know if \mathbf{D} is generated by a tree, its corresponding tree must be able to be reduced to a depth-1 tree by absorption. In such case, each node matches with one edge, such that for each row or column, there is only one element is 1. Property 1

Property 1: *Rows and columns of \mathbf{D} are interchangeable.*

shows such matrix can be rearranged to an permutation matrix by switching rows and columns with their labels.

$\mathbf{I} \Rightarrow t$:

Assuming there is a matrix $\mathbf{D} \notin \mathbb{D}_N$ but can be reduced to a permutation matrix by a sequence s of the two operations. Such operation must has a corresponding depth-1 tree in \mathbb{T}_N . We know the inverse operation of switching rows is switching rows (the same pair), the inverse operation of switching columns is switching columns. Dilation and absorption are inverse operation for each other. So by proposition 3, in domain \mathbb{T}_N , there should be a reversed sequence \bar{s} that grows a depth-1 tree. Corollary 1

Corollary 1: *Tree set \mathbb{T}_N is closed under dilation and absorption.*

shows such grown tree should also be a heterogeneous out-tree. By lemma 1,

Lemma 1: *From each heterogeneous out-tree, one can extract a determined heterogeneous dependency matrix.*

such tree is equivalent to a matrix in \mathbb{D}_N . Due from proposition 4,

Proposition 4: *The tree to matrix translation in Lemma 1 is bijective.*

such tree only have one corresponding matrix $\mathbf{D} \in \mathbb{D}_N$, it is contradictory to $\mathbf{D} \notin \mathbb{D}_N$. So such \mathbf{D} does not exist.
end of proof.

APPENDIX L PROOF OF PROPOSITION 5

We first prove a lemma and its corollary.

Lemma 4. *If $\mathbf{D} \in \{0,1\}^{n \times n}$ satisfies $\{1^\circ, 5^\circ\}$, then for any $r \in \text{row}(\mathbf{D})$, there exists a $c \in \text{col}(\mathbf{D})$ such that $r \in J_{S_c}$.*

Proof: For any $r \in \text{row}(\mathbf{D})$, by 1° , there exist $c \in \text{col}(\mathbf{D})$ such that $r \in S_c$. From all the columns c that "includes" row r , we pick the c with the minimum number of elements,

which is $c_{min} = \arg \min_{c \in \text{col}(\mathbf{D}), r \in S_c} |S_c|$. By 5°, such c_{min} is unique. Because if we have another column c' , there are three cases:

1) $S_{c_{min}} \subseteq S_{c'}$, in such case, $|S_{c'}| \geq |S_{c_{min}}|$, equality holds when $S_{c'} = S_{c_{min}}$. So, as we shall pick the set with minimum number of elements, we will still pick $S_{c_{min}}$ unless they are the same (where it is still unique).

2) $S_{c_{min}} \supseteq S_{c'}$. In this case, because c_{min} can be chosen arbitrarily, we can choose c' as the new c_{min} , which is still unique.

3) $S_{c_{min}} \cap S_{c'} = \emptyset$, apparently $r \notin S_{c'}$

As it has the minimum number of elements, S_c cannot have a proper set that also includes row r (though it can still have proper sets). Thus, r only belongs to c but not to any proper set of c , $r \in J_{S_c}$.

end of proof.

Corollary 2. Each row r in $\mathbf{D} : \{1^\circ, 5^\circ, 6^\circ\}$ or $\mathbf{D} : \{1^\circ, 3^\circ, 5^\circ\}$ corresponds to a unique J_{S_c} .

Proof: 1) If $\mathbf{D} : \{1^\circ, 5^\circ, 6^\circ\}$: Assuming two rows r_1, r_2 correspond to the same J_{S_c} , we will have $|J_{S_c}| \geq 2$, which violates 6°.

2) If $\mathbf{D} : \{1^\circ, 3^\circ, 5^\circ\}$: Assuming two rows r_1, r_2 correspond to the same J_{S_c} , we discuss the relation between S_c and another column set $S_{c'}$. Due to 5°, there are following relations:

1) $S_c \subseteq S_{c'}$: both r_1, r_2 belong to $S_{c'}$.

2) $S_c \supset S_{c'}$: both r_1, r_2 not belong to $S_{c'}$.

3) $S_c \cap S_{c'} = \emptyset$: both r_1, r_2 not belong to $S_{c'}$.

4) $S_c = S_{c'}$: both r_1, r_2 belong to $S_{c'}$.

So for any $S_{c'} \neq S_c$, r_1, r_2 simultaneously belong to or not belong to $S_{c'}$, which means r_1 and r_2 are equivalent, which violates 3°

end of proof.

Proposition 5 A matrix $\mathbf{D} \in \{0,1\}^{n \times n}$ satisfies $P_0 \Leftrightarrow \mathbf{D}$ satisfies P .

Proof: Such proposition is equivalent to prove $\{6^\circ\} \Leftrightarrow \{3^\circ, 4^\circ\}$.

“ \Rightarrow ”: Let matrix \mathbf{D} satisfies P_0 , which has $r_1, r_2 \in \text{row}(\mathbf{D}), r_1 \neq r_2, c_1, c_2 \in \text{col}(\mathbf{D}), c_1 \neq c_2$. What we show is when 3° or 4° does not hold, 6° does not hold.

1) When 3° not holds: Assume $r_1 = r_2$, e.e., then for any $c \in \text{col}(\mathbf{D})$, r_1 and r_2 must be simultaneously present or absent in S_c . Then by Lemma 4, r_1, r_2 must be simultaneously present in $J_{S_c}, \exists c' \in \text{col}(\mathbf{D})$, contradicts with condition 6°, that each J_{S_c} can only has one element. Thus, 3° must hold.

2) When 4° not holds: Assume $c_1 = c_2$, e.e., we must have $J_{S_{c_1}} = J_{S_{c_2}}$, which violates corollary 2 that J_{S_c} for all rows are unique. Thus, 4° must hold.

“ \Leftarrow ”: Let matrix \mathbf{D} satisfies P and assume 6° does not hold. We discuss two different cases of violation of 6° separately:

1) If there exists c such that $|J_{S_c}| \geq 2$, due to corollary 2's proof, it leads to violation to 3°

2) If there exists c such that $|J_{S_c}| < 1$, by Lemma 4, there are totally n rows belongs to $n-1$ non-empty Unique Element Sets (eliminate column c), implying at least one of J_{S_c} have at least 2 rows, which is the same case as $|J_{S_c}| \geq 2$.

end of proof.

APPENDIX M

DEMONSTRATION OF MATRIX TO OUT-TREE TRANSLATION ALGORITHM

We show a demonstration of running the algorithm in Figure 20. Assuming we have a heterogeneous matrix

$$\mathbf{D} = \begin{bmatrix} 1 & 0 & 1 & 1 & 0 \\ 1 & 0 & 0 & 0 & 0 \\ 1 & 0 & 1 & 0 & 1 \\ 1 & 0 & 1 & 0 & 0 \\ 1 & 1 & 0 & 0 & 0 \end{bmatrix} \quad (44)$$

with row labels $\{a, b, c, d, f\}$ and column labels $\{e_1, e_2, e_3, e_4, e_5\}$. The row set r is the result of decomposing matrix \mathbf{D} by rows, $r = \{[1, 0, 1, 1, 0], [1, 0, 0, 0, 0], [1, 0, 1, 0, 1], [1, 0, 1, 0, 0], [1, 1, 0, 0, 0]\}$, explored set $E = \emptyset$. We can calculate the depths of a, b, c, d, f as the sum of their corresponding rows $r_a = 3, r_b = 1, r_c = 3, r_d = 2, r_f = 2$.

step 1: pick the node with minimum depth $r_{min} = r_b$. As the depth $r_b = 1$, we directly attach b to the root node. In r_b , the column label with '1' indicates the parent edge of b , which is e_1 . Remove r_b from r and add it to E .

step 2: pick the node with minimum depth $r_{min} = r_d$ (also can pick f , does not affect the result). Search in E , where r_d has one more '1' than any row in E . it gives r_b , which means node d should be a child of node b . The unique '1' r_d compared with r_b indicates the parent edge of d , which is e_3 . Remove r_d from r and add it to E .

step 3: pick the node with minimum depth $r_{min} = r_f$. Search in E , where r_f has one more '1' than any row in E . it gives r_b , which means node f should be a child of node b . The unique '1' r_f compared with r_b indicates the parent edge of f , which is e_2 . Remove r_f from r and add it to E .

step 4: pick the node with minimum depth $r_{min} = r_a$. Search in E , where r_a has one more '1' than any row in E . it gives r_d , which means node a should be a child of node d . The unique '1' r_a compared with r_d indicates the parent edge of a , which is e_4 . Remove r_a from r and add it to E .

step 5: pick the node with minimum depth $r_{min} = r_c$. Search in E , where r_c has one more '1' than any row in E . it gives r_d , which means node c should be a child of node d . The unique '1' r_c compared with r_d indicates the parent edge of c , which is e_5 . Remove r_c from r and add it to E .

return: heterogeneous out-tree.

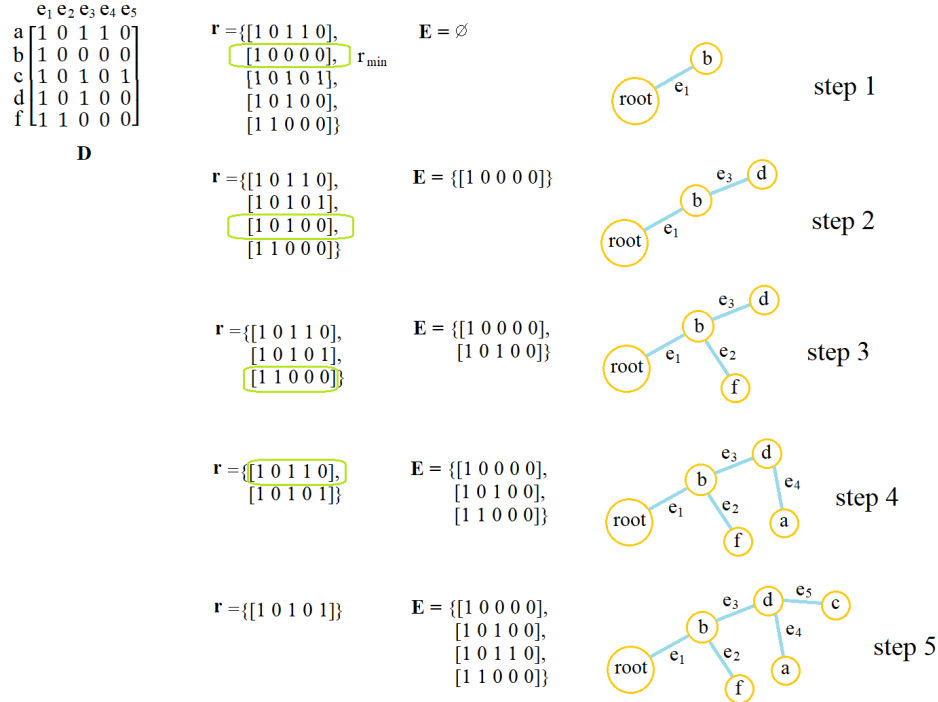


Fig. 20: Demonstration of Matrix to Out-tree Translation Algorithm.

APPENDIX N PROOF OF THEOREM 2

Theorem 2 D : $P \Leftrightarrow \mathbf{D}$ can be grown to a heterogeneous out-tree.

Proof: “ \Rightarrow ”: The meaning of J_{S_c} is the node’s label which is the direct child of column c (or edge c). $|J_{S_c}| = 1$ indicates for each edge, its direct child has been determined. Thus, we can extract N different pairs of “edge-node” from such \mathbf{D} . We can construct such tree by first attaching all edges that has maximum $|S_c|$ to the root. Then attach the edges with S_c which has no intersection to other $S_{c'}$ also to the root. For any column c left, whose S_c must be a subset of some $S_{c'}$ that already connected to the root, because we have already attached all the edges whose S_c share no intersection to others, that is the third case in 5°. Then we can attach the rest c by a decreasing order of $|S_c|$ to the tree, specifically to c' that $S_c \subseteq S_{c'}$. In such way, we can generate a tree from $\mathbf{D} : P$.

“ \Leftarrow ”: From Lemma 1

Lemma 1: From each heterogeneous out-tree, one can extract a determined heterogeneous dependency matrix.

we know for a heterogeneous out-tree, there is a \mathbf{D} can be generated. We show such \mathbf{D} fulfills condition set P .

1°: An all-0 row means a node that has no path to the root, it is not allowed in out-tree.

2°: An all-0 column means an edge with no descendent node, such open edge is not allowed in out-tree.

3°: Duplicate rows indicates the same node, which can

be merged when constructing \mathbf{D} without changing tree’s topology.

4°: Duplicate columns indicates the two sub-trees rooted at the two edges include the same set of nodes. As it is a tree structure, such sub-tree can only have one path to the root, which means the edges should be the same edges, they can still be merged.

5°: If a node a whose parent edge is θ_1 , is the descendent of another node b whose parent edge is θ_2 , there should be $S_{c\theta_1} \subseteq S_{c\theta_2}$. If b is a descendent of a , then $S_{c\theta_1} \supseteq S_{c\theta_2}$. If a, b are not on the same branch, apparently $S_{c1} \cap S_{c2} = \emptyset$. Because there cannot be a case that S_{c1} and S_{c2} share some intersections, at least for some common nodes in the two sub-trees from edges θ_1 and θ_2 , the nodes has two parents θ_1 and θ_2 .

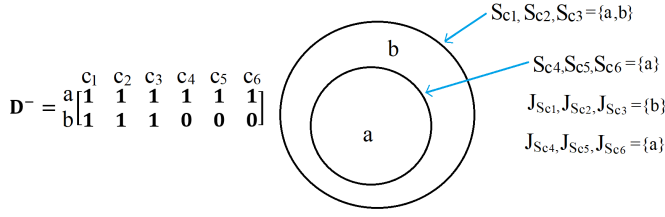
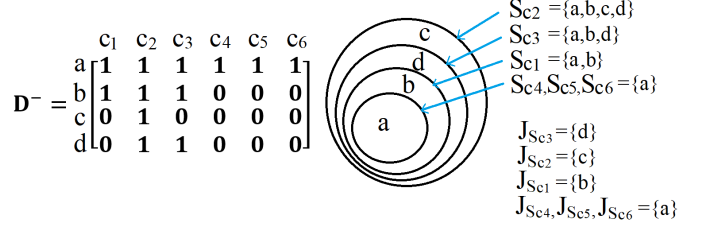
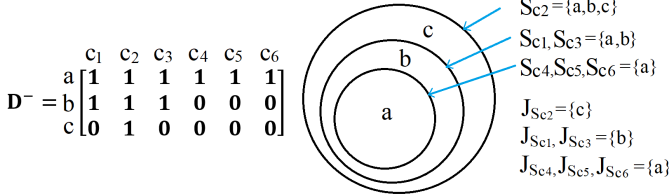
end of proof.

APPENDIX O MATRIX COMPLETION ALGORITHM EXAMPLE

We use an example here to show how such algorithm works. Considering matrix

$$\mathbf{D}^- = \begin{bmatrix} 1 & 1 & 1 & 1 & 1 & 1 \\ 1 & 1 & 1 & 0 & 0 & 0 \end{bmatrix} \quad (45)$$

Such matrix can be extracted from robot with 6 joints (number of columns) and 2 sensors (two rows). One sensor depends on all 6 joints (it is mounted on the arm extremity) and the other sensor only depends on only the first three joints (it is mounted on the third link). There are 4 links that with no sensor mounted, so they are unobservable. The complete form of such matrix should be 6×6 , because in fully observable

Fig. 21: D^- (left) and D^- in S_c space (right)Fig. 23: D^- (left) and D^- in S_c space (right)Fig. 22: D^- (left) and D^- in S_c space (right)

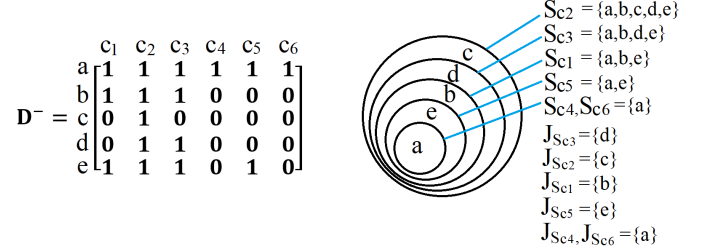
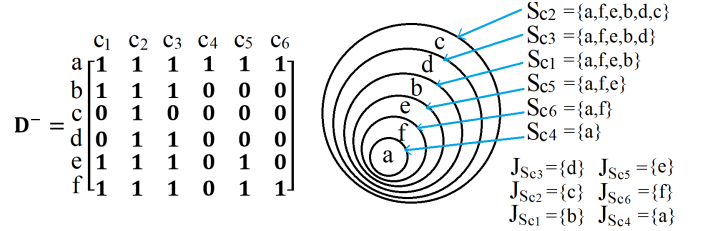
case, each link is at least with one sensor mounted, and 6 joints correspond to 6 links except root. So we assume the original fully-observable matrix is 6×6 . We can assign any name to rows and columns, e.g., we assign rows as $[a, b, c, d, e, f]$ and columns $[c_1, c_2, c_3, c_4, c_5, c_6]$. Among these, rows c, d, e, f are not observable. It is easy to find D^- fulfills P^- , so there has to be a way to fill it to a $D : P$ of size $N \times N$. We draw D^- in S_c space with S_c and J_{S_c} for each column in Figure 21.

We now have two sets with K unique J_{S_c} , as c_1, c_2, c_3 have the same J_{S_c} and c_4, c_5, c_6 have the same J_{S_c} . We can pick one with $|J_{S_c}| > 0$ from each set, e.g., $\{c_1, c_4\}$. The rest of other columns becomes another set $\{c_2, c_3, c_5, c_6\}$. According to Corollary 2, J_{S_c} of different columns should be different, which is not true for now, we need to assign dependency of unused nodes to the columns in set $\{c_2, c_3, c_5, c_6\}$ to make J_{S_c} unique. Also, we have a set of unused nodes $\{c, d, e, f\}$.

Then for each column in $\{c_2, c_3, c_5, c_6\}$, we find a unused node (a row) in unused set $\{c, d, e, f\}$ and assign dependency to the column c_i and all c_j s as S_{c_j} is the proper super-set of S_{c_i} . For example, we first have c_2 , and pick one node from unused node set, e.g. node c . Then We add dependency of c with c_2 and columns that have proper super-set of S_{c_2} . From Figure 21, we see, S_{c_2} has no proper super-set. So the new matrix and new S_c representation becomes Figure 22:

Eliminating c and c_2 from sets above, we have to pick a new pair from $\{c_3, c_5, c_6\}$ and $\{d, e, f\}$. Let us pick c_3 and d . Then we can add dependency of d with c_3 and columns that have proper super-set of S_{c_3} . From Figure 22, we see the proper super-set of S_{c_3} is S_{c_2} , so we add a new row to D^- , the result is shown in Figure 23

Eliminating d and c_3 from sets above, we have to pick a new pair from $\{c_5, c_6\}$ and $\{e, f\}$. Let us pick c_5 and e . Then we add dependency of e with c_5 and columns that have proper super-set of S_{c_5} . From Figure 22, we see the proper super-set of S_{c_5} are S_{c_1} , S_{c_2} and S_{c_3} , so we add a new row to D^- , the result is shown in Figure 24

Fig. 24: D^- (left) and D^- in S_c space (right)Fig. 25: D^- (left) and D^- in S_c space (right)

Eliminating e and c_5 from sets above, we only have c_6 and f . Then we add dependency of f with c_6 and columns that have proper super-set of S_{c_6} . From Figure 23, we see the proper super-set of S_{c_6} are S_{c_1} , S_{c_2} , S_{c_5} and S_{c_3} , so we add a new row to D^- , the result is shown in Figure 25. Until now, we have successfully filled the $N \times N$ matrix. Reader can check such matrix is under condition set P .

APPENDIX P PROOF OF THEOREM 3

Lemma 5. If we have $D^- : P^-$, for any column c in D^- , $|J_{S_c}| \leq 1$

Proof: We prove it by showing when there is a column c that $|J_{S_c}| \geq 2$, P^- will be violated. If $|J_{S_c}| \geq 2$, there are two rows belong to the same J_{S_c} , this is equivalent to corollary 2's proof 2) case, it violates condition 3 $^\circ$ in P^- . end of proof.

Corollary 3. If we have $D^- : P^-$, there exists K columns that $|J_{S_c}| = 1$ and the J_{S_c} are unique.

Proof: Because there are K non-all-0 rows, by Lemma 4,

Lemma 4: If $\mathbf{D} \in \{0, 1\}^{n \times n}$ satisfies $\{1^\circ, 5^\circ\}$, then for any $r \in \text{row}(\mathbf{D})$, there exists a $c \in \text{col}(\mathbf{D})$ such that $r \in J_{S_c}$.

there must be K non-empty J_{S_c} . Also by Lemma 5, the J_{S_c} have $|J_{S_c}| \leq 1$. Because they are non-empty, $|J_{S_c}| = 1$. So each J_{S_c} only contains one row, and for every J_{S_c} , they are different.
end of proof.

Theorem 3 A $\mathbf{D}^- : P^-$ can be filled to a $\mathbf{D} : P$. Such filling is unique when $N - K = 1$ and there is one J_{S_c} is \emptyset .

Proof: “ \Leftarrow ”: If the original \mathbf{D} fulfills P , the sub-matrix \mathbf{D}^- must fulfill P^- . As \mathbf{D}^- is a sub-matrix of $\mathbf{D} : P$, we consider which conditions in P is inherited to P^- . A sub-matrix is to eliminate several rows in original matrix. Because rows are independent, all the conditions for rules are inherited, $1^\circ, 3^\circ$. Eliminating rows will cause columns to lose some elements, it is possible to create duplicate or all-0 columns, so $2^\circ, 4^\circ$ do no more apply. Apparently if in original matrix if we have 5° , the three relations $S_{c1} \subseteq S_{c2}$, $S_{c1} \supseteq S_{c2}$, $S_{c1} \cap S_{c2} = \emptyset$ in 5° should also fit in \mathbf{D}^- . Thus, $P^- = \{1^\circ, 3^\circ, 5^\circ\}$.

“ \Rightarrow ”: As we demonstrate a constructive algorithm in this section to fill \mathbf{D}^- , we only need to show the completed \mathbf{D} is under condition P or P_0 . From Corollary 3 we know initially there are K non-all empty rows, and there can be all-zero columns. As we pick K columns at the first step of the algorithm with unique J_{S_c} , the rest $N - K$ columns should have the same J_{S_c} with one of the picked K columns (because $|J_{S_c}| \leq 1$ by Lemma 5) or it is empty. That means we have to assign the rest $N - K$ unused nodes to the $N - K$ columns to make their J_{S_c} different from the picked K columns, that ensures condition 1° and 2° . In S_c space, it is equivalent to assign nodes to the overlapped S_c sets or sets with no J_{S_c} . As in Figure 25, the sets should be non-intersection and has its only one J_{S_c} node, which ensures condition 6° . As we only extend overlapping S_c sets or sets with no J_{S_c} , which ensures condition 5° . Thus, the completed \mathbf{D} is under condition set P_0 , equivalently P .

Because we have to assign $N - K$ nodes to $N - K$ columns, there are different ways of such assignment. The permutation causes the assignment not unique. Such uniqueness is only fulfilled by assign one node to one column, that is $N - K = 1$. Also there should be one J_{S_c} is \emptyset , because if J_{S_c} is not \emptyset , c must be a duplicate column (has the same S_c) of some column c' in the picked K columns. As the two columns are indistinguishable, one can pick either c or c' in the first K columns, that causes two different assignments. Thus, the ununiqueness comes from two sources, one is picking duplicate columns in the first K columns, the second is assign the rest $N - K$ unused nodes to the $N - K$ columns.
end of proof.

$$\begin{bmatrix} 1 & 1 & 0 \\ 0 & 1 & 1 \\ 1 & 0 & 1 \end{bmatrix} \xrightarrow{\text{MILP}} \begin{bmatrix} 1 & 0 & 0 \\ 0 & 1 & 0 \\ 0 & 0 & 1 \end{bmatrix}$$

Fig. 26: \mathbf{D} and \mathbf{I} by MILP

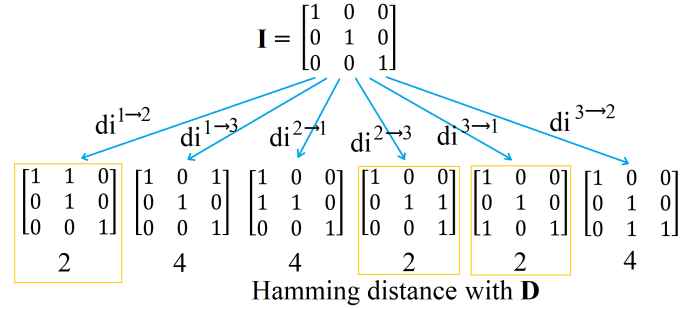


Fig. 27: One-step dilation result from Trellis algorithm. Yellows are optimal candidates of \mathbf{D}^-

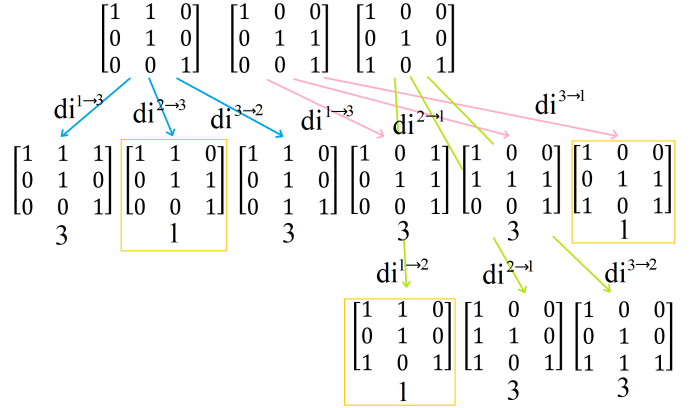


Fig. 28: One-step dilation result from Trellis algorithm.

APPENDIX Q MATRIX CORRECTION ALGORITHM EXAMPLE

We use an example to show how the algorithm works. The original matrix \mathbf{D} and \mathbf{I} calculated by MILP are shown in Figure 26. It generates the most similar permutation matrix \mathbf{I} to the original matrix \mathbf{D} .

We then generate all possible one-step dilation matrices as in Figure 27, calculate their Hamming distance to \mathbf{D} and pick the matrices with smallest Hamming distance (yellow ones). Running one more step dilation will lead to Figure 28. The minimal Hamming distance now reduce to 1. Continuing with more dilation operations will not reduce the Hamming distance anymore, so the algorithm stops at this step. There are three candidate matrices with equal Hamming distances, we can pick any of these as the correct matrix. For a partially observed matrix \mathbf{D}^- , we can first fill it to a $N \times N$ matrix by set all missing elements as zero and then perform the correction algorithm.

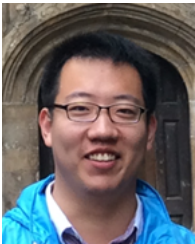
REFERENCES

- [1] Sers, Ryan, et al. "Validity of the Perception Neuron inertial motion capture system for upper body motion analysis." *Measurement* 149 (2020): 107024.

- [2] Ly, Daniel L., Ashutosh Saxena, and Hod Lipson. "Co-evolutionary predictors for kinematic pose inference from rgbd images." *Proceedings of the 14th annual conference on Genetic and evolutionary computation*. 2012.
- [3] Bongard, J. C., Victor Zykov, and Hod Lipson. "Automated synthesis of body schema using multiple sensor modalities." *Proc. of the Int. Conf. on the Simulation and Synthesis of Living Systems (ALIFEX)*. 2006.
- [4] Chen, Boyuan, et al. "Fully body visual self-modeling of robot morphologies." *Science Robotics* 7.68 (2022): eabn1944.
- [5] Sturm, Jürgen, Christian Plagemann, and Wolfram Burgard. "Body schema learning for robotic manipulators from visual self-perception." *Journal of Physiology-Paris* 103.3-5 (2009): 220-231.
- [6] Fang, Bin, et al. "3D human gesture capturing and recognition by the IMMU-based data glove." *Neurocomputing* 277 (2018): 198-207.
- [7] Pan, Tse-Yu, et al. "Multisensor-based 3D gesture recognition for a decision-making training system." *IEEE Sensors Journal* 21.1 (2020): 706-716.
- [8] Choe, Namchol, et al. "A sensor-to-segment calibration method for motion capture system based on low cost MIMU." *Measurement* 131 (2019): 490-500.
- [9] Naeemabadi, MReza, et al. "Influence of a marker-based motion capture system on the performance of Microsoft Kinect v2 skeleton algorithm." *IEEE Sensors Journal* 19.1 (2018): 171-179.
- [10] Van der Kruk, Eline, and Marco M. Reijne. "Accuracy of human motion capture systems for sport applications; state-of-the-art review." *European journal of sport science* 18.6 (2018): 806-819.
- [11] Zenha, Rodrigo, et al. "Incremental adaptation of a robot body schema based on touch events." *2018 Joint IEEE 8th International Conference on Development and Learning and Epigenetic Robotics (ICDL-EpiRob)*. IEEE, 2018.
- [12] Li, Qiang, Robert Haschke, and Helge Ritter. "Towards body schema learning using training data acquired by continuous self-touch." *2015 IEEE-RAS 15th International Conference on Humanoid Robots (Humanoids)*. IEEE, 2015.
- [13] Vicente, Pedro, Lorenzo Jamone, and Alexandre Bernardino. "Online body schema adaptation based on internal mental simulation and multisensory feedback." *Frontiers in Robotics and AI* 3 (2016): 7.
- [14] Cunha, Gonçalo, et al. "Online Body Schema Adaptation through Cost-Sensitive Active Learning." *arXiv preprint arXiv:2101.10892* (2021).
- [15] Martinez-Cantin, Ruben, Manuel Lopes, and Luis Montesano. "Body schema acquisition through active learning." *2010 IEEE international conference on robotics and automation*. IEEE, 2010.
- [16] Head, Henry, and Gordon Holmes. "Sensory disturbances from cerebral lesions." *Brain* 34.2-3 (1911): 102-254.
- [17] Hoffmann, Matej, et al. "Body schema in robotics: a review." *IEEE Transactions on Autonomous Mental Development* 2.4 (2010): 304-324.
- [18] Kalman, Rudolph Emil. "A new approach to linear filtering and prediction problems." (1960): 35-45.
- [19] Bullard, Sarah E., et al. "Encyclopedia of clinical neuropsychology." (2013): 92-92.
- [20] Mittendorfer, Philipp, Emmanuel Dean, and Gordon Cheng. "Automatic robot kinematic modeling with a modular artificial skin." *2014 IEEE-RAS International Conference on Humanoid Robots*. IEEE, 2014.
- [21] Mimura, Tomohiro, et al. "Bayesian body schema estimation using tactile information obtained through coordinated random movements." *Advanced Robotics* 31.3 (2017): 118-134.
- [22] Carter, Rita. *The human brain book: An illustrated guide to its structure, function, and disorders*. Penguin, 2019.
- [23] Görür, Dilan, and Carl Edward Rasmussen. "Dirichlet process gaussian mixture models: Choice of the base distribution." *Journal of Computer Science and Technology* 25.4 (2010): 653-664.
- [24] Flor, Herta. "Phantom-limb pain: characteristics, causes, and treatment." *The Lancet Neurology* 1.3 (2002): 182-189.
- [25] Ota, J, Naito, E. "Understanding brain plasticity on body representations to promote their adaptive functions-Embodied brain systems science" *World Engineering Conference and Convention (WECC2015)*.
- [26] Bullard, Sarah E and Griss, Mélina and Greene, Sonia and Gekker, Anna "Encyclopedia of clinical neuropsychology" *Oxford University Press* 2013.
- [27] Carter, Rita and Aldridge, S and Page, M and Parker, S "The human brain book: An illustrated guide to its structure, function, and disorders" *New York: DorlingKindersley Limited* 2009.
- [28] Jun Ota, Eiichi Naito, etc. "Understanding brain plasticity on body representations to promote their adaptive functions-Embodied brain systems science" *Proceedings of World Engineering Conference and Convention (WECC2015)*.
- [29] Rogelio Guadarrama Olvera, J and Leon, Emmanuel Dean and Bergner, Florian and Cheng, Gordon "Plantar tactile feedback for biped balance and locomotion on unknown terrain" *International Journal of Humanoid Robotics*, 17-01-1950036, 2020, World Scientific.
- [30] Jiang, Shuo and Wong, Lawson LS "Active Tactile Exploration using Shape-Dependent Reinforcement Learning" *2022 IEEE/RSJ International Conference on Intelligent Robots and Systems (IROS)*
- [31] Chen, Boyuan and Kwiatkowski, Robert and Vondrick, Carl and Lipson, Hod "Fully body visual self-modeling of robot morphologies" *Science Robotics*, 7-68-eabn1944, 2022



Shuo Jiang Shuo Jiang studied control, Microsystems and Microelectronics at the University of Bremen, Germany, and received the M.Sc. degree in 2018. Currently, he is working towards the Ph.D. degree at the Northeastern University, USA. His research interests lie in the areas of robot tactile perception, robot body schema learning.



Jinkun Zhang Jinkun Zhang studied Microelectronics at the Fudan University, and received the B.Sc. degree in 2017. Currently, he is working towards the Ph.D. degree at the Northeastern University, USA. His research interests lie in the areas of network optimization, distributed storage and distributed computing.



Lawson L.S. Wong Lawson L.S. Wong is an assistant professor in the Khoury College of Computer Sciences at Northeastern University. His research focuses on learning, representing, and estimating knowledge about the world that an autonomous robot may find useful. Prior to Northeastern, Lawson was a postdoctoral fellow at Brown University. He completed his PhD at the Massachusetts Institute of Technology. He has received a Siebel Fellowship, AAAI Robotics Student Fellowship, and Croucher Foundation Fellowship for Postdoctoral Research.